

# Performance Analysis of RIS-Assisted Full-Duplex Communications with Infinite and Finite Blocklength Codes

Keshav Singh, *Member, IEEE*, Farjam Karim, Sandeep Kumar Singh, *Member, IEEE*, Prabhat Kumar Sharma, *Senior Member, IEEE*, Shahid Mumtaz, *Senior Member, IEEE*, and Mark F. Flanagan, *Senior Member, IEEE*

**Abstract**—With the advancement of wireless communication technologies, reconfigurable intelligent surfaces (RISs) have recently paved the way to augmenting the performance of wireless networks with the aid of multiple reflecting surfaces by efficiently attuning the signal reflection through a large number of low-cost passive elements. In this paper, we consider an RIS-aided full-duplex (FD) communication network consisting of a FD access point (AP) that communicates with an uplink and a downlink user simultaneously with the aid of an RIS as well as through the direct link between the AP and users. To evaluate the system performance under infinite blocklength (IBL) and finite blocklength (FBL) codes, we derive the analytical expressions for the outage probability and throughput in case of IBL, and for block-error rate (BLER) and goodput in the case of FBL, for both uplink and downlink transmission. Furthermore, the expressions for the maximum achievable rate under FBL and IBL transmission are derived. Next, we also extend the analysis of the single-user framework to a more practical scenario with multiple users utilizing non-orthogonal multiple access (NOMA) and derive analytical expressions for the outage probability and BLER at each downlink user and at the AP. The accuracy of the derived expressions is validated via simulation results, and insights are provided regarding the impact of the number of reflecting elements and imperfect channel state information (CSI) on the performance of the considered system. Finally, from the comparative analysis, it is shown that the RIS-aided system outperforms the system without RIS in both IBL and FBL scenarios, providing remarkable improvement in the outage probability and BLER.

**Index Terms**—Reconfigurable intelligent surface (RIS), full-duplex (FD), finite block length (FBL), outage probability, uplink, downlink, throughput, block-error rate (BLER), goodput.

## I. INTRODUCTION

The work of K. Singh was supported by the National Science and Technology Council of Taiwan, under Grant NSTC 111-3114-E-110-001. The work of M. F. Flanagan was supported by the Irish Research Council under Grant IRCLA/2017/209. (*Corresponding author: Keshav Singh.*)

Keshav Singh and Sandeep Kumar Singh are with the Institute of Communications Engineering, National Sun Yat-sen University, Kaohsiung 80424, Taiwan, R.O.C. (e-mail: {keshav.singh,sks }@mail.nsysu.edu.tw).

Farjam Karim was with International Master's Program in Telecommunication Engineering (IMPTE), National Sun Yat-sen University, Kaohsiung 80424, Taiwan, R.O.C. (e-mail: farjamkarim@g-mail.nsysu.edu.tw)

P. K. Sharma is with the Department of Electronics and Communication Engineering, Visvesvaraya National Institute of Technology, Nagpur 440010, India (e-mail: prabhatmadhavec1@gmail.com).

Shahid Mumtaz is with the Department of Engineering, Nottingham Trent University, UK (e-mail: shahid.mumtaz@ntu.ac.uk).

Mark F. Flanagan is with the School of Electrical and Electronic Engineering, University College Dublin, Ireland. (e-mail: mark.flanagan@ieee.org).

THE last few years have seen a dramatic growth in the number of wireless devices as well as an increase in the demand for ubiquitous wireless network connectivity and higher data rate. It has become essential to take effective measures to meet the demands of connected devices which are exponentially increasing with time. Consequently, research scholars around the world have made great efforts to investigate novel and ultra-modern wireless communication technologies [1], [2]. Reconfigurable intelligent surface (RIS) assisted communication has emerged off as an efficient alternative to conventional relaying. It uses a discrete set of meta-material reflecting surfaces to assist the communication between wireless devices such as cellular users (CUs), access points (APs), etc. The primary reason for its growing popularity among researchers is its capability to enhance the signal quality with very low power consumption and thereby provide better achievable diversity, higher data rate and a more reliable system [3], [4]. Moreover, an RIS can easily be coupled to or decoupled from existent objects in the environment such as ceilings and building walls, and can be perfectly incorporated into cellular or WiFi systems without altering their current functional installations and operating standards [5], [6]. Thus, it is an emerging technology which can have a very high impact on the performance of communication systems. The numerous advantages of RIS have motivated great interest in analysing RIS reflection beamforming designs in diverse RIS-aided wireless systems [7]–[9]. On a similar note, another technological advancement called full-duplex (FD) communication has the potential to improve the spectral efficiency of the system by transmitting and receiving the signal simultaneously using the same resources [10], [11]. Therefore, the integration of the RIS into FD communication systems has been well motivated by researchers [12]–[14] in order to achieve low power reliable RIS-assisted transmission with an efficient use of the available resources. The authors in [14] have presented a clear demonstration of the difference in the achievable rate of FD and half-duplex (HD) systems.

While most existing research works have considered a single RIS [8], the use of multiple RISs in wireless communication has also been well motivated by researchers in [15]–[18]. For instance, the authors in [15] used multiple-RISs in a device-to-device (D2D) FD communication system and derived a closed-form expression for the outage probability. In [17] the authors analyzed the performance of a multiple-RIS-aided downlink

cellular system where the average signal-to-interference-plus-noise ratio (SINR) was maximized by optimizing passive beamforming at each RIS. Likewise, in [19] the performance of an intelligent reflecting surface (IRS) aided single input single output (SISO) communication system assuming a direct link between transmitter and receiver was analysed. In order to achieve higher spectral efficiency, the authors in [20] considered an RIS-assisted multi-user uplink communication system in which a virtual constellation diagram is devised by the RIS to transmit the data of an extra user. The authors in [18] analyzed the performance of a multi-RIS-aided system for the case of infinite blocklength (IBL) without deriving the closed-form expression of the performance metrics. Note that the above existing works considered IBL transmission; however, the analysis of IBL codes cannot directly apply to the case of finite blocklength (FBL) codes. Moreover, performance indicators such as outage capacity and Shannon capacity do not provide an accurate estimation of the maximum achievable rate when the blocklength is small, making the IBL analysis insufficient for analyzing the performance during FBL transmission; hence, the need arises for a more accurate analysis approach for FBL transmission.

The advancement of 5G and beyond 5G (B5G) communication necessitates more rapid services like pervasive connectivity, remote surgery, industrial automation, extended reality (XR) and tactile communications with stringent specifications resulting in the emergence of new key performance indicators such as end-to-end latency, reliability, cycle time, typical payload size and coverage. For example, wearables or exoskeletons for healthcare applications has a low latency requirement of ( $< 20$  ms) and block error rate (BLER)  $10^{-5}$ - $10^{-6}$  [21], for industrial automation motion control the cycle time and typical payload sizes are ( $< 2$  ms, 20 bytes), ( $< 0.5$  ms, 50 bytes) and ( $< 1$  ms, 40 bytes) for printing machine, machine tool and packaging machine respectively [22]. Short packet transmission has emerged as a prospective transmission technology to fulfill these severe requirements for real-time transmission and its use has been well explained in [23]–[25]. However, there will be a severe decline in the channel gain because of the receiver errors, which makes it challenging for communication reliability as well as end-to-end Quality of Service (delay) requirements. A comprehensive analysis for reliability performance considering FBL and IBL transmissions of a nonlinear energy harvesting unmanned aerial vehicle assisted FD Internet of Things (IoT) network has been investigated in [25]. In [26], the performance of relaying under the FBL regime as well as under the Shannon capacity regime was examined, and it was shown that relaying outperforms direct transmission under the FBL regime even if their performances are similar under the Shannon capacity regime. One of the important obstacles to the application of short-packet communications is to provide highly reliability. In [27], the authors investigated how reliability and security can be guaranteed in the presence of an eavesdropper in short packet communication. Moreover, in [28], the authors studied two user-antenna selection methods considering two clusters of users having different priority levels for short packet communication in non-orthogonal multiple access (NOMA)-

assisted multiuser downlink multiple input multiple output (MIMO) systems, and analyzed the minimum blocklength for Nakagami- $m$  fading channels. It is noteworthy that there is a lack of relevant analytical framework in the literature and the advantages of using an RIS in FD communications are yet to be explored. *Therefore, the main focus of this work is to study the impact of the RIS on an FD cellular communication system in the FBL transmission regime.*

#### A. Motivation and Contributions

Motivated by the performance-enhancing potential of the RIS-aided FD wireless communication system, it is of high interest to analyze the performance of the considered system model. In contrast to conventional relay-based technologies, the RIS can passively reflect the incident signal, thus enhancing the system's throughput, diversity and energy efficiency. Moreover, to the best of the authors' knowledge, none of the recent related works has studied the performance analysis of RIS-aided FD communication with IBL and FBL transmission, which is the main focus of this work. Hence, in this work, we study an RIS-aided FD communication network wherein a FD-AP acts as a base station and communicates with an uplink and a downlink user simultaneously with the aid of two RISs, one for each link. The main contributions of this paper are as follows:

- We first derive the characteristics of the SINR during each transmission and evaluate its probability distribution function (PDF) using the central limit theorem (CLT) and moment matching (MM) approximation methods, showing that both methods provide the same performance. Specifically, we derive these characteristics considering that both AP-RIS-user and BS-user links follow a Nakagami- $m$  distribution in the presence of imperfect SI cancellation.
- Next, we investigate the performance of the considered system under two different transmission schemes: 1) IBL transmission, and 2) FBL transmission. We analyze the performance of each link in terms of BLER and goodput for FBL transmission, and outage probability and throughput for IBL transmission. Moreover, we derive closed-form expressions for these performance metrics using the characteristics of the respective SINRs. Furthermore, we derive expressions for the achievable rate at each device in both FBL and IBL scenarios.
- Then, using the aforementioned single-user framework, we extend the analysis to a more practical case with multiple users utilizing NOMA in each link, and we derive analytical expressions for the outage probability and BLER at each downlink user and at the AP.
- We validate the accuracy of the derived analytical expressions using Monte-Carlo simulation. We find that the use of the RIS in such networks provides an additional degree of freedom to achieve the desired QoS by increasing the number of reflecting elements at each RIS. Furthermore, we also compare the achievable rate performance of the IBL and FBL transmissions. In addition to this, we highlight the trade-off between the downlink transmit

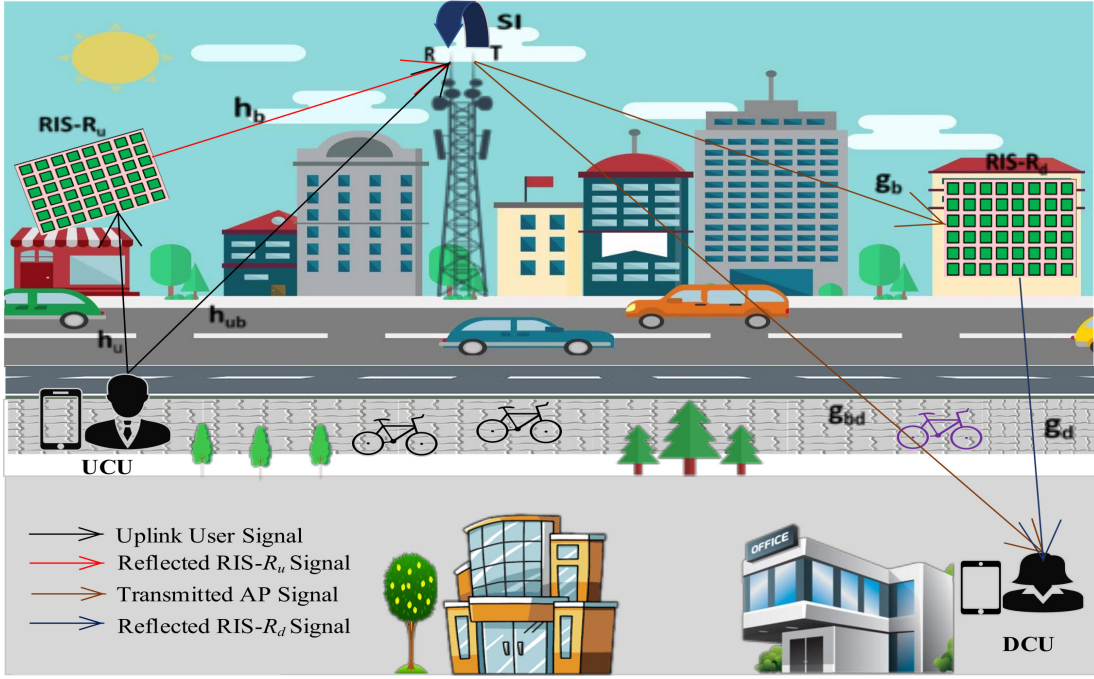


Fig. 1: An illustration of RIS-aided FD communication system.

power and achievable rates (uplink and downlink) during FBL transmission.

- We also highlight the impact of CSI estimation error on the performance of the considered network, and we demonstrate the importance of a judicious choice of the number of RIS elements in the presence of this error to achieve a desired QoS. Moreover, we discuss the impact of the number of users on the average outage probability in the multi-user case.

**Organization:** The flow of this paper is organized as follows. Section II provides a detailed explanation of the considered system model. In section III and IV, SINR characteristics in terms of PDF and CDF, closed-form expressions for BLER, goodput for FBL transmission and outage probability are derived. In Section V, the achievable rate for FBL and IBL transmission are derived. Section VI discussed the extension to the multi-user case. Simulation results are discussed in Section VII and finally, the conclusions are drawn in Section VIII.

**Notations:** Matrices, vectors and scalars are denoted by boldface upper case, boldface lower case and lower case letters, respectively. Also,  $\mathcal{CN}(0, \sigma^2)$  denotes the complex Gaussian distribution with zero mean and variance  $\sigma^2$ .  $f_Z(z)$  and  $F_Z(z)$  denote the PDF and cumulative distribution function (CDF), respectively, of the random variable  $Z$ .  $K_{(\cdot)}(\cdot)$  represents the modified Bessel function of the second kind.  $(\cdot)^H$  represents the Hermitian transpose of a matrix or vector.

## II. SYSTEM MODEL

This work considers a FD communication system, as illustrated in Fig. 1, which is comprised of an AP, which is working as a base station, two RISs, an uplink CU (UCU)

and a downlink CU (DCU). Each of the CUs is equipped with a single antenna and operates in HD mode. The AP operates in FD mode using a single transmit and a single receive antenna to communicate simultaneously with the DCU and UCU, respectively. Further, due to severe fading/pathloss in the direct path between the respective device pairs, two RISs are used (one for each link) to assist this wireless information transfer<sup>1</sup>. In particular, the UCU transmits its information uplink to the AP with the aid of the RIS ( $R_u$ ) having  $K$  reflecting elements ( $\mathcal{K} \in \{1, 2, \dots, K\}$ ) and at the same time the AP transmits its information downlink to the DCU using the RIS ( $R_d$ ) having  $N$  reflecting elements ( $\mathcal{N} \in \{1, 2, \dots, N\}$ ).

### A. Channel Model

In the uplink,  $h_{ub}$  represents the channel gain of the direct path between UCU and AP. Also, the channel between UCU and the  $k^{\text{th}}$  element of  $R_u$  is denoted by  $h_{uk}$ . Thus, the vector of channel gains between the UCU and  $R_u$  is denoted by  $\mathbf{h}_u = [h_{u1}, h_{u2}, \dots, h_{uK}]^H$ . Similarly, the channel gains between  $R_u$  and AP is denoted by  $\mathbf{h}_b = [h_{1b}, h_{2b}, \dots, h_{Kb}]^H$  where  $h_{kb}$  depicts the gain between the  $k^{\text{th}}$  element of  $R_u$  and AP with  $k \in \mathcal{K}$ . Further,  $\Theta = \text{diag}[e^{j\theta_1}, \dots, e^{j\theta_K}]$  represents the phase shift matrix at  $R_u$  with  $\theta_k \in [0, 2\pi)$  denoting the phase shift of the  $k^{\text{th}}$  element. Correspondingly, in the downlink, the channel between AP and  $R_d$  is expressed as  $\mathbf{g}_b = [g_{b1}, g_{b2}, \dots, g_{bn}]^H$  with  $g_{bn}$  representing the channel gain between AP and the  $n^{\text{th}}$  element of  $R_d$ . Additionally, the channel between  $R_d$  and DCU is denoted by  $\mathbf{g}_d = [g_{1d}, g_{2d}, \dots, g_{Nd}]^H$  with  $g_{nd}$  representing the channel

<sup>1</sup>Based on the product-distance path loss model [29], we can infer that the average received signal power through the “AP-RIS- $R_u$ -DCU” link and the “UCU-RIS- $R_d$ -AP” link is negligible.

gain between the  $n^{\text{th}}$  element of  $R_d$  and DCU with  $n \in \mathcal{N}$ . Furthermore,  $g_{bd}$  is the channel coefficient for the direct path between AP and DCU.  $\Phi = \text{diag}[e^{j\phi_1}, \dots, e^{j\phi_N}]$  depicts the phase shift matrix at  $R_d$  with  $\phi_n \in [0, 2\pi)$  denoting the phase shift of the  $n^{\text{th}}$  element. Due to the non-line of sight (nLoS) nature of the direct link between AP and CUs, we assume  $h_{ub}$  and  $g_{bd}$  follow  $\mathcal{CN}(0, \sigma^2)$  and therefore their magnitudes are Rayleigh distributed [19], [30], [31] with a PDF of

$$f_Y(y) = ye^{-y^2/2}, \quad (1)$$

where  $Y \in \{h_{ub}, g_{bd}\}$ . However, due to LoS nature of the links between the RIS and the devices, we assume  $h_{uk}$ ,  $h_{kb}$ ,  $g_{bn}$  and  $g_{nd}$  follow Nakagami- $m$  fading [32]–[35]. Via the  $m$  parameter, the Nakagami- $m$  model can cover both severe and weak fading, and includes Rayleigh fading as a special case. It can also closely approximate the Hoyt and Rice distributions, and is therefore widely used in analyzing the performance of RIS-assisted wireless networks. Its PDF is given by [36]

$$f_{X_i}(x) = \frac{2m_i^{m_i}}{\Gamma(m_i)\Omega_i^{m_i}} x^{2m_i-1} \exp\left(-\frac{m_i}{\Omega_i}x^2\right), \quad (2)$$

where  $X \in \{h, g\}$ ,  $i \in \{uk, kb, bn, nd\}$ , and  $m_i$  and  $\Omega_i$  denote the shape and spread parameters of the respective channel. Also, without loss of generality, all channels are assumed to be independent and identically distributed. Further, we assume perfect CSI acquisition and feedback information among the respective devices with no hardware impairments<sup>2</sup>.

### B. Information Transfer

The UCU transmits the unit-energy information symbol  $s_u$  to the AP using transmit power  $P_u$  and the corresponding signal received at the AP is given by

$$y_u = \underbrace{(\mathbf{h}_b^H \Theta \mathbf{h}_u + h_{ub})\sqrt{P_u} s_u}_{\text{desired signal}} + \underbrace{g_{bb}\sqrt{P_b} s_d}_{\text{SI}} + \underbrace{n_b}_{\text{AWGN}}, \quad (3)$$

where  $n_b \sim \mathcal{CN}(0, \sigma^2)$  denotes the additive white Gaussian noise (AWGN).  $g_{bb} \sim \mathcal{CN}(0, \psi_{si})$  denotes the self-interference (SI) channel and  $s_d$  is the unit-energy symbol transmitted from AP to DCU (the transmit power used is  $P_b$ ). The SINR to decode  $s_u$  from  $y_u$  can be expressed as

$$\begin{aligned} \gamma_u &= \frac{|\mathbf{h}_b^H \Theta \mathbf{h}_u + h_{ub}|^2 \frac{P_u}{(\sigma^2 + P_{SI})}}{\left| \sum_{k \in \mathcal{K}} h_{uk} h_{kb} e^{j\theta_k} + h_{ub} \right|^2 \frac{P_u}{(\sigma^2 + P_{SI})}}, \quad (4) \end{aligned}$$

<sup>2</sup>Note that CSI estimation in RIS-aided networks can be performed using some standard algorithms such as parallel factor decomposition [37]. Therefore, similar to [13], [15], [38], we assume perfect CSI in this paper for analytical tractability. Although very important, the analysis of a RIS-assisted network with channel and hardware related impairments (such as training overhead, imperfect estimation, control signaling, etc.) is an extremely complex and challenging task, and lies beyond the scope of this paper. However, for useful insights, we highlight the impact of CSI estimation error on the performance of the considered network in Fig. 18 and Fig. 19 of Section VII.

where  $P_{SI} = \rho |\psi_{si}|^2 P_u$  is the power of the residual SI<sup>3</sup> with  $\rho \in [0, 1]$  denoting the residual SI cancellation factor. Further, as mentioned earlier, AP is operating in FD mode, therefore, along with receiving the signal from UCU, AP also transmits the unit energy symbol  $s_d$  to DCU. The signal received at DCU can be expressed as

$$y_d = \underbrace{\mathbf{g}_d^H \Phi \mathbf{g}_b \sqrt{P_b} s_d + g_{bd} \sqrt{P_b} s_d}_{\text{desired signal}} + \underbrace{n_d}_{\text{AWGN}}, \quad (5)$$

where  $n_d \sim \mathcal{CN}(0, \sigma^2)$  is the AWGN. The signal-to-noise ratio (SNR) required at DCU for decoding  $s_d$  from  $y_d$  is given by

$$\begin{aligned} \gamma_d &= \frac{|\mathbf{g}_d^H \Phi \mathbf{g}_b + g_{bd}|^2 P_b / \sigma^2}{\left| \sum_{n \in \mathcal{N}} g_{bn} g_{nd} e^{j\phi_n} + g_{bd} \right|^2 P_b / \sigma^2}. \quad (6) \end{aligned}$$

### III. SINR CHARACTERISTICS

As discussed earlier, the AP receives the uplink information from UCU with an SINR of  $\gamma_u$ , given in (4). We derive the PDF of  $\gamma_u$  in the following Lemma:

**Lemma 1.** *The approximate PDF of the SINR  $\gamma_u$  is given by (7), which is given on the top of the next page, where*

$\mu_{h_r} = K \left( \frac{\Omega_1 \Omega_2}{m_1 m_2} \right)^{\frac{1}{2}} \frac{\Gamma(m_1 + 0.5) \Gamma(m_2 + 0.5)}{\Gamma(m_1) \Gamma(m_2)}$ ,  $\sigma_{h_r}^2 = K \Omega_1 \Omega_2 - \frac{\mu_{h_r}^2}{K}$ ,  $a = \sqrt{\gamma \alpha} - \mu_{h_r}$ ,  $q = \frac{1 + \sigma_{h_r}^2}{2\sigma_{h_r}^2}$ ,  $v = a / \sigma_{h_r}^2$  and  $\alpha = (P_{SI} + \sigma^2) / P_u$ .  $m_1$  and  $\Omega_1$  are the shape and spread parameter of  $h_{uk}$ ,  $\forall k \in \mathcal{K}$ , while  $m_2$  and  $\Omega_2$  are the shape and spread parameter of  $h_{kb}$ ,  $\forall k \in \mathcal{K}$ . Note that the accuracy of (7) increases with increasing  $K$ .

*Proof.* To evaluate the PDF of  $\gamma_u$ , we first simplify (4) as

$$\gamma_u = \frac{\left| \sum_{k \in \mathcal{K}} |h_{uk}| |h_{kb}| \exp(-j(\theta_{uk} + \theta_{kb} - \theta_k)) + h_{ub} \right|^2 P_u}{(\sigma^2 + P_{SI})}, \quad (8)$$

where  $\theta_{uk}$  and  $\theta_{kb}$  denote the angle of  $h_{uk}$  and  $h_{kb}$ , respectively. Now, as shown in [41], [42], the SINR is maximized at  $\theta_{uk} + \theta_{kb} = \theta_k$ . Therefore, we also evaluate the PDF considering  $\theta_{uk} + \theta_{kb} = \theta_k \forall k \in \mathcal{K}$ . Next, we define  $h_k \triangleq |h_{uk}| |h_{kb}|$ , and considering the independence of  $|h_{uk}|$  and  $|h_{kb}|$ , we evaluate the PDF of  $h_k$  as

$$f_{h_k}(z) = \int_0^\infty (1/y) f_{|h_{uk}|}(y) f_{|h_{kb}|}(z/y) dy. \quad (9)$$

Using (2), we can write

$$\begin{aligned} f_{h_k}(z) &= \int_0^\infty \frac{2m_1^{m_1} y^{2m_1-1}}{\Gamma(m_1) \Omega_1^{m_1}} \exp\left(-\frac{m_1}{\Omega_1} y^2\right) \frac{2m_2^{m_2} (z/y)^{2m_2-1}}{\Gamma(m_2) \Omega_2^{m_2}} \\ &\quad \times \exp\left(-\frac{m_2}{\Omega_2} \frac{z^2}{y}\right) \frac{1}{y} dy, \quad (10) \end{aligned}$$

where  $\{m_{uk} = m_1, m_{kb} = m_2, \Omega_{uk} = \Omega_1, \Omega_{kb} = \Omega_2\} \forall k \in \mathcal{K}$ ,  $\{m_{bn} = m_3, m_{nd} = m_4, \Omega_{bn} = \Omega_3, \Omega_{nd} = \Omega_4\} \forall n \in \mathcal{N}$ .

<sup>3</sup>A significant amount of SI can be eliminated using standard methods such as analog and digital SI cancellation techniques [39], [40]. Therefore, residual SI power is very low compared to that of the received signal, and is often modelled as a constant in performance analysis.

$$f_{\gamma_u}(\gamma) \simeq \frac{\exp\left(\frac{-a^2}{2\sigma_{h_r}^2} - \frac{v^2}{4q^2}\right)}{2q\sqrt{2\pi\sigma_{h_r}^2\gamma\alpha}} \left[ \Gamma\left(1, \frac{v^2}{4q}\right) - \Gamma\left(1, q\left(\sqrt{\gamma\alpha} - \frac{v}{2q}\right)^2\right) + \frac{v}{2\sqrt{q}} \left( \Gamma\left(\frac{1}{2}, \frac{v^2}{4q}\right) - \Gamma\left(\frac{1}{2}, q\left(\sqrt{\gamma\alpha} - \frac{v}{2q}\right)^2\right) \right) \right]. \quad (7)$$

Using an approach similar to that of [15], we solve (10) to obtain

$$f_{h_k}(z) = S_1 z^{m_1+m_2-1} K_{m_1-m_2} \left( 2z\sqrt{\frac{m_1 m_2}{\Omega_1 \Omega_2}} \right), \quad (11)$$

where  $S_1 = \frac{4m_1^{m_1} m_2^{m_2}}{\Gamma(m_1)\Gamma(m_2)\Omega_1^{m_1}\Omega_2^{m_2}} \left(\frac{m_2\Omega_1}{m_1\Omega_2}\right)^{\frac{m_2-m_1}{2}}$ . Using (11) and the central limit theorem (CLT), for large  $K$  the PDF of  $h_r \triangleq \sum_{k=1}^K h_k$  can be closely approximated as a Gaussian distribution with mean  $\mu_{h_r}$  and variance  $\sigma_{h_r}^2$ , which can be expressed as

$$f_{h_r}(y) = \frac{1}{\sigma_{h_r}\sqrt{2\pi}} \exp\left(-\frac{(y-\mu_{h_r})^2}{2\sigma_{h_r}^2}\right). \quad (12)$$

Next, defining  $Z_u = |h_r + h_{ub}|$ , and using (1) and (12), we obtain the PDF of  $Z_u$  as

$$f_{Z_u}(z) = \int_0^z \frac{y}{\sqrt{2\pi\sigma_{h_r}^2}} \exp\left(-\frac{(z-y-\mu_{h_r})^2}{2\sigma_{h_r}^2} - \frac{y^2}{2}\right) dy. \quad (13)$$

After some mathematical simplification, we have

$$f_{Z_u}(z) = \frac{\exp\left(\frac{-a^2}{2\sigma_{h_r}^2}\right)}{\sqrt{2\pi\sigma_{h_r}^2}} \int_0^z y \exp(-qy^2 + vy) dy. \quad (14)$$

Solving (14) using [43, 3.326.4], we obtain the PDF of  $Z_u$  as (15) on top of the next page.

Fig. 2 compares the derived PDF in (15) of the variable  $Z_u$  with its PDF obtained using simulation. It can be seen that the analytical and simulated PDFs are very similar, which validates the accuracy of Lemma 1 as well as the approximations used to obtain (15). Further, it can also be observed that the accuracy is greater at higher values of  $K$  as compared to lower values of  $K$ . The reason for this behaviour is the CLT approximation considered in (12), which becomes more accurate as the number of elements  $K$  increases. Using the PDF of  $Z_u$ , we can express the PDF of  $Z_u^2$  as (16), which is given on top of the next page. Further, from (8), the PDF of the SINR  $\gamma_u$  in terms of the PDF of  $Z_u^2$  is expressed as

$$f_{\gamma_u}(\gamma) = f_{Z_u^2}(\gamma\alpha). \quad (17)$$

Using (16) and (17), we obtain (7). ■

Further, we would like to highlight that due to the non-LoS nature of the direct link, Rayleigh channels are widely adopted for analyzing the system performance in RIS-assisted networks. However, in order to enhance the generality of our analysis, we also derive the PDF of the SINR  $\gamma_u$  considering the direct path as a Nakagami- $m$  channel in the following lemma.

**Lemma 2.** *The PDF of the SINR  $\gamma_u$  when  $h_{ub}$  follows a Nakagami- $m$  distribution can be approximated as*

$$f_{\gamma_u}(\gamma) \simeq \frac{2m_5^{m_5} e^{-\frac{a^2}{2\sigma_{h_r}^2}}}{\Gamma(m_5)\Omega^{m_5}\sqrt{2\gamma\alpha\pi\sigma_{h_r}^2}} \times \left( \frac{\sqrt{\gamma\alpha}^{2m_5}}{2m_5} - \frac{q\sqrt{\gamma\alpha}^{2m_5+2}}{2m_5+2} - \frac{v\sqrt{\gamma\alpha}^{2m_5+1}}{2m_5+1} \right), \quad (18)$$

where  $m_5$  and  $\Omega_5$  are the shape and spread parameter of  $h_{ub}$ , respectively.

*Proof.* We first consider that, instead of a Rayleigh distribution,  $h_{ub}$  follows a Nakagami- $m$  distribution with shape and spread parameters  $m_5$  and  $\Omega_5$ , respectively. Thus, re-evaluating the PDF of  $Z_u = |h_r + h_{ub}|$  in (13), we obtain

$$f_{Z_u}(z) = \frac{2m_5^{m_5} e^{-\frac{a^2}{2\sigma_{h_r}^2}}}{\Gamma(m_5)\Omega^{m_5}\sqrt{2\pi\sigma_{h_r}^2}} \times \int_0^z y^{2m_5-1} \exp(-qy^2 + vy) dy. \quad (19)$$

Using  $e^{-ax} \approx (1 - ax)$  [43], we obtain

$$f_{Z_u}(z) = \frac{2m_5^{m_5} e^{-\frac{a^2}{2\sigma_{h_r}^2}}}{\Gamma(m_5)\Omega^{m_5}\sqrt{2\pi\sigma_{h_r}^2}} \times \int_0^z (qy^{2m_5-1} - y^{2m_5+1} + vy^{2m_5}) dy = \frac{2m_5^{m_5} e^{-\frac{a^2}{2\sigma_{h_r}^2}}}{\Gamma(m_5)\Omega^{m_5}\sqrt{2\pi\sigma_{h_r}^2}} \times \left( \frac{z^{2m_5}}{2m_5} - \frac{qz^{2m_5+2}}{2m_5+2} - \frac{vz^{2m_5+1}}{2m_5+1} \right). \quad (20)$$

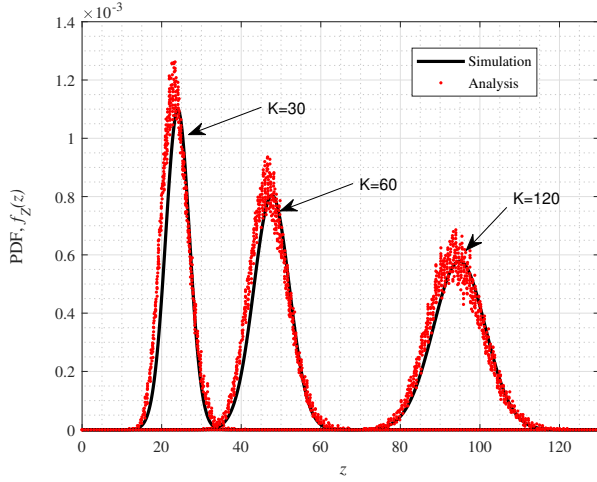
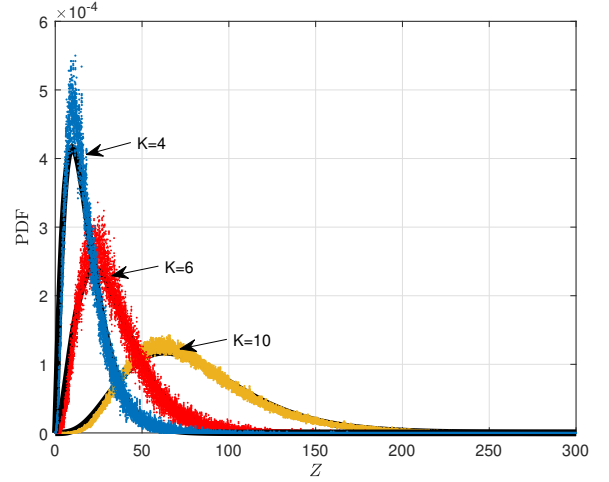
Substituting (20) into (17), we obtain (18). ■

Note that although the CLT has a higher accuracy, it requires a large number of elements to provide an accurate expression. Thus, the moment matching (MM) method can alternatively be adopted to approximate the PDF of  $Z_u^2$  in (16). It is noteworthy that a non-negative random variable (RV)  $Y$  with first and second moments given by  $\mu_Y$  and  $\mu_Y^{(2)}$ , respectively, can be approximated as a Gamma RV ( $\mathbb{G}$ ) i.e.  $Y \sim \mathbb{G}(\kappa, \nu)$  where  $\kappa = \frac{\mu_Y^2}{\mu_Y^{(2)} - \mu_Y^2}$  represents the shape and  $\nu = \frac{\mu_Y^{(2)} - \mu_Y^2}{\mu_Y}$  represents the scale parameters [44]. Thus, the PDF and CDF of  $Y$  can be expressed as [45]

$$f_Y(y) = (\kappa/\nu)^\kappa y^{\kappa-1} e^{-(\kappa/\nu)y} / \Gamma(\kappa),$$

$$f_{Z_u}(z) = \frac{\exp\left(\frac{-a^2}{2\sigma_{h_r}^2} - \frac{v^2}{4q^2}\right)}{q\sqrt{8\pi\sigma_{h_r}^2}} \left[ \Gamma\left(1, \frac{v^2}{4q}\right) - \Gamma\left(1, q\left(z - \frac{v}{2q}\right)^2\right) + (v/2\sqrt{q})\Gamma\left(\frac{1}{2}, q\left(-\frac{v}{2q}\right)^2 - (v/2\sqrt{q})\Gamma\left(\frac{1}{2}, q\left(z - \frac{v}{2q}\right)^2\right)\right) \right]. \quad (15)$$

$$f_{Z_u^2}(z) = \frac{\exp\left(\frac{-a^2}{2\sigma_{h_r}^2} - \frac{v^2}{4q^2}\right)}{q\sqrt{8z\pi\sigma_{h_r}^2}} \left[ \Gamma\left(1, \frac{v^2}{4q}\right) - \Gamma\left(1, q\left(\sqrt{z} - \frac{v}{2q}\right)^2\right) + (v/2\sqrt{q})\Gamma\left(\frac{1}{2}, q\left(-\frac{v}{2q}\right)^2\right) - (v/2\sqrt{q})\Gamma\left(\frac{1}{2}, q\left(\sqrt{z} - \frac{v}{2q}\right)^2\right) \right]. \quad (16)$$

Fig. 2: PDF of  $Z_u$  using CLTFig. 3: PDF of  $Z_u$  using MM method

$$F_Y(y) = \gamma(\kappa, \nu)/\Gamma(\kappa), \quad (21)$$

where  $\gamma$  represents the lower incomplete Gamma function [46]. For analytical simplicity, we assume  $\Omega_i = 1 \forall i \in \{1, 2, \dots, 6\}$ . Therefore, in contrast to the CLT used in (12), similar to [44],  $h_r$  can be approximated as Gamma RV given by

$$h_r \sim \mathbb{G}\left(K \frac{\mu_u^2}{1 - \mu_u^2}, \frac{1 - \mu_u^2}{\mu_u}\right), \quad (22)$$

where  $\mu_u = \frac{\Gamma(m_1 + \frac{1}{2})\Gamma(m_2 + \frac{1}{2})}{\Gamma(m_1)\Gamma(m_2)(m_1 m_2)^{1/2}}$ . The mean and variance of  $h_r$  are given by  $\mu_{h_r}^{(1)} = K\mu_u, \mu_{h_r}^{(2)} - \mu_{h_r}^2 = K(1 - \mu_u^2)$ . Since,  $Z_u^2 = |h_r + h_{ub}|^2$ , the first and second moments of  $Z_u^2$  can be expressed as  $\mu_{Z_u} = \mu_{h_{ub}}^{(2)} + \mu_{h_r}^{(2)} + 2\mu_{h_{ub}}\mu_{h_r}, \mu_{Z_u}^{(2)} = \mu_{h_{ub}}^{(4)} + \mu_{h_r}^{(4)} + 6\mu_{h_{ub}}^{(2)}\mu_{h_r}^{(2)} + 4\mu_{h_{ub}}^{(3)}\mu_{h_r} + 4\mu_{h_{ub}}\mu_{h_r}^{(3)}$ , where  $\mu_{h_{ub}}^{(p)} = \frac{\Gamma(m_5 + \frac{p}{2})}{\Gamma(m_5)(m_5)^{p/2}}, \mu_{h_r}^{(p)} = \frac{\Gamma(K\kappa_{h_r} + p)(\nu_{h_r})^p}{\Gamma(K\kappa_{h_r})}, \kappa_{h_r} = \frac{\mu_u^2}{1 - \mu_u^2}, \nu_{h_r} = \frac{\mu_u^{(2)} - \mu_u^2}{\mu_u}$ . Using  $\mu_{Z_u}, \mu_{Z_u}^{(2)}$  and the MM method,  $Z_u^2$  can be approximated as

$$Z_u^2 \sim \mathbb{G}(\kappa_{Z_u}, \nu_{Z_u}), \quad (23)$$

where  $\kappa_{Z_u} = \frac{\mu_{Z_u}^2}{\mu_{Z_u}^{(2)} - \mu_{Z_u}^2}, \nu_{Z_u} = \frac{\mu_{Z_u}^{(2)} - \mu_{Z_u}^2}{\mu_{Z_u}}$ . The PDF and CDF of  $Z_u^2$  can be obtained by substituting  $\kappa = \kappa_{Z_u}$  and  $\nu = \nu_{Z_u}$  in (21). For explicit clarity, we verify the accuracy of the MM method by plotting the PDF of  $Z_u$ , obtained using (23), in Fig. 3. As can be seen, the approximation holds very well even in the case of a small number of RIS elements. Moreover, we also highlight the difference between the approximation accuracy of the MM and CLT methods by comparing Fig. 2 and Fig. 3. It can be seen that the approximation is in very close agreement in the case of the MM method even when  $K = 4$ , in contrast to the CLT based method which requires  $K > 30$  elements to have similar accuracy. Thus, from (21), the PDF of  $\gamma_u$  using the MM method can be evaluated as

$$f_{\gamma_u}^{\text{MM}}(y) = (\kappa_{Z_u}/\nu_{Z_u})^{\kappa_{Z_u}} (\alpha y)^{\kappa_{Z_u} - 1} e^{-(\kappa_{Z_u}/\nu_{Z_u})\alpha y} / \Gamma(\kappa_{Z_u}). \quad (24)$$

Note that the aforementioned equations are derived when, due to its NLoS nature, the SI channel follows Rayleigh fading. However, for the LoS case, it follows a Rician distribution and the corresponding PDF of SINR is given in the following lemma.

**Lemma 3.** The PDF of  $\gamma_u$  when  $g_{bb}$  follows a Rician distribution is approximately given by (25), which is given on top of the next page, where  $I_{(\cdot)}$  is the modified Bessel function of the first kind with order  $r$  and  $\nu$  denotes the number of degrees of freedom,  $\mu_{hr} = K \left( \frac{\Omega_1 \Omega_2}{m_1 m_2} \right)^{\frac{1}{2}} \frac{\Gamma(m_1+0.5)\Gamma(m_2+0.5)}{\Gamma(m_1)\Gamma(m_2)}$ ,  $\sigma_{hr}^2 = K\Omega_1\Omega_2 - \frac{\mu_{hr}^2}{K}$ ,  $a(x) = \sqrt{\gamma\alpha(x) - \mu_{hr}}$ ,  $q = (1 + \sigma_{hr}^2)/(2\sigma_{hr}^2)$ ,  $\lambda = \mu_{hr}/\sigma_{hr}^2$ ,  $v(x) = a(x)/\sigma_{hr}^2$ , and  $\alpha(x) = (P_b x + \sigma^2)/P_u$ .

*Proof.* To evaluate the PDF of  $\gamma_u$ , we first simplify the uplink SINR as

$$\gamma_u = \frac{\left| \sum_{k \in \mathcal{K}} |h_{uk}| |h_{kb}| \exp(-j(\theta_{uk} + \theta_{kb} - \theta_k)) + h_{ub} \right|^2 P_u}{P_b |g_{bb}|^2 + \sigma^2}, \quad (26)$$

where  $g_{bb}$  is the SI channel which follows a Rician distribution and the PDF of its absolute square ( $|g_{bb}|^2$ ) follows a non-central Chi-square distribution [45]. Thus, (25) can be obtained by substituting  $P_{SI} = P_b |g_{bb}|^2$  and averaging (16) over the PDF of  $|g_{bb}|^2$ . Note that, due to the extremely complex nature of (25), finding its closed-form expression seems to be intractable. ■

**Lemma 4.** The PDF of the SNR  $\gamma_d$  is approximately given by (27), which is given on top of the next page, where

$\mu_{gr} = N \left( \frac{\Omega_3 \Omega_4}{m_3 m_4} \right)^{\frac{1}{2}} \frac{\Gamma(m_3+0.5)\Gamma(m_4+0.5)}{\Gamma(m_3)\Gamma(m_4)}$ ,  $\sigma_{gr}^2 = N\Omega_3\Omega_4 - \frac{\mu_{gr}^2}{N}$ ,  $p = \gamma\beta - \mu_{gr}$ ,  $t = \frac{1+\sigma_{gr}^2}{2\sigma_{gr}^2}$ ,  $w = p/\sigma_{gr}^2$ ,  $\beta = \sigma^2/P_b$ ,  $m_3$  and  $\Omega_3$  are the shape and spread parameter of  $g_{bn}$  for all  $n \in \mathcal{N}$ ,  $m_4$  and  $\Omega_4$  are the shape and spread parameter of  $g_{nd}$  for all  $n \in \mathcal{N}$ .

*Proof.* To evaluate the PDF of  $\gamma_d$ , we first simplify (6) as

$$\gamma_d = (P_b/\sigma^2)|g_{bd} + \sum_{n \in \mathcal{N}} |g_{bn}| |g_{nd}| \exp(-j(\phi_{bn} + \phi_{nd} - \phi_n))|^2, \quad (28)$$

where  $\phi_{bn}$  and  $\phi_{nd}$  denote the angle of  $g_{bn}$  and  $g_{nd}$ , respectively. Similar to (8), we evaluate the PDF of  $\gamma_d$  considering  $(\phi_{bn} + \phi_{nd} = \phi_n) \forall n \in \mathcal{N}$ . Next, we assume  $Z_d = \left| \sum_{n \in \mathcal{N}} |g_{bn}| |g_{nd}| + g_{bd} \right|^2$ . Note that the PDF of  $Z_d^2$ ,  $f_{Z_d^2}(z)$ , can be evaluated using steps similar to those used to obtain (16). Furthermore, from (28), the PDF of the SINR  $\gamma_d$  can be expressed in terms of the PDF of the channel gain  $Z_d^2$  via

$$f_{\gamma_d}(\gamma) = f_{Z_d^2}(\gamma\beta). \quad (29)$$

Using (16) and (29), we obtain (27). ■

Similarly, considering  $g_{bd}$  as Nakagami distributed, the PDF of the SNR  $\gamma_d$  is given by

$$f_{\gamma_d}(\gamma) \simeq \frac{2m_6^{m_6} \exp\left(\frac{-p^2}{2\sigma_{gr}^2}\right)}{\Gamma(m_6)\Omega^{m_6} \sqrt{2\gamma\beta\pi\sigma_{gr}^2}} \times \left( \frac{\sqrt{\gamma\beta}^{2m_5}}{2m_5} - \frac{t\sqrt{\gamma\beta}^{2m_6+2}}{2m_6+2} - \frac{w\sqrt{\gamma\beta}^{2m_6+1}}{2m_6+1} \right), \quad (30)$$

where  $m_6$  and  $\Omega_6$  are the shape and spread parameter of  $g_{bd}$ .

Further, using an approach similar to (24), the PDF<sup>4</sup> of  $\gamma_d$  using the MM method can be evaluated as

$$f_{\gamma_d}^{\text{MM}}(y) = \frac{(\kappa_{Z_d}/\nu_{Z_d})^{\kappa_{Z_d}} (\beta y)^{\kappa_{Z_d}-1}}{\Gamma(\kappa_{Z_d})} e^{-(\kappa_{Z_d}/\nu_{Z_d})\beta y}, \quad (31)$$

where  $\kappa_{Z_d} = \frac{\mu_{Z_d}^2}{\mu_{Z_d}^{(2)} - \mu_{Z_d}^2}$ ,  $\nu_{Z_d} = \frac{\mu_{Z_d}^2 - \mu_{Z_d}^2}{\mu_{Z_d}}$ ,  $\mu_{Z_d} = \mu_{g_{bd}}^{(2)} + \mu_{g_r}^{(2)} + 2\mu_{g_{bd}}\mu_{g_r}$ ,  $\mu_{Z_d}^{(2)} = \mu_{g_{bd}}^{(4)} + \mu_{g_r}^{(4)} + 6\mu_{g_{bd}}^{(2)}\mu_{g_r}^{(2)} + 4\mu_{g_{bd}}^{(3)}\mu_{g_r} + 4\mu_{g_{bd}}^{(3)}\mu_{g_r}^{(3)}$ ,  $\mu_{g_{bd}}^{(p)} = \frac{\Gamma(m_6 + \frac{p}{2})}{\Gamma(m_6)(m_6)^{p/2}}$ ,  $\mu_{g_r}^{(p)} = \frac{\Gamma(N\kappa_{g_r} + p)(\nu_{g_r})^p}{\Gamma(N\kappa_{g_r})}$ ,  $\kappa_{g_r} = \frac{\mu_{g_r}^2}{\mu_{g_r}^{(2)} - \mu_{g_r}^2}$ ,  $\nu_{g_r} = \frac{\mu_{g_r}^2 - \mu_{g_r}^2}{\mu_{g_r}}$ ,  $\mu_{g_r}^{(1)} = N\mu_d$ ,  $\mu_{g_r}^{(2)} - \mu_{g_r}^2 = N(1 - \mu_d^2)$ ,  $\mu_d = \frac{\Gamma(m_3 + \frac{1}{2})\Gamma(m_4 + \frac{1}{2})}{\Gamma(m_3)\Gamma(m_4)(m_3 m_4)^{1/2}}$ ,  $\Omega_3 = \Omega_4 = \Omega_6 = 1$ .

## IV. PERFORMANCE ANALYSIS

In this section, we derive closed-form expressions for the BLER and goodput for the case of FBL transmission, and for outage probability and throughput for the case of IBL transmission.

### A. Finite Block Length Analysis

#### 1) Uplink BLER

Let  $\varphi_{b_u}$  be the overall BLER of the uplink of the considered RIS-assisted network, assuming that the UCU transmits  $a_{sp}$  information bits in  $\varpi_s$  channel uses (i.e., the blocklength of the channel code is  $\varpi_s$ ). Thus the code rate (in bits per channel use) is given by  $r_{b_u} = a_{sp}/\varpi_s$ . When  $\varpi_s$  is reasonably large ( $> 100$ ), the BLER can be tightly approximated as [47], [48]

$$\varphi_{b_u} \approx \mathbb{E} \left\{ Q \left( \frac{C(\gamma_u) - r_{b_u}}{\sqrt{V(\gamma_u)/\varpi_s}} \right) \right\}, \quad (32)$$

where  $C(\gamma_u) = \log_2(1 + \gamma_u)$  is the Shannon capacity and  $V(\gamma_u) = (1 - (1 + \gamma_u)^{-2})(\log_2 e)^2$  is the channel dispersion which measures the stochastic variability of the channel relative to a deterministic channel with the same capacity [13], [49].

**Theorem 1.** The achievable uplink BLER at the AP can be approximated by (33), which is given on top of the

next page, where  $\mu_{hr} = K \left( \frac{\Omega_1 \Omega_2}{m_1 m_2} \right)^{\frac{1}{2}} \frac{\Gamma(m_1+0.5)\Gamma(m_2+0.5)}{\Gamma(m_1)\Gamma(m_2)}$ ,  $\sigma_{hr}^2 = K\Omega_1\Omega_2 - \frac{\mu_{hr}^2}{K}$ ,  $a = (\xi_{b_u} + \zeta_{b_u})\alpha - \mu_{hr}$ ,  $q = \frac{1+\sigma_{hr}^2}{2\sigma_{hr}^2}$ ,  $v = \frac{a}{\sigma_{hr}^2}$ ,  $\alpha = \frac{(PSI + \sigma^2)}{P_u}$ ,  $\vartheta_{b_u} = \frac{1}{2\pi\sqrt{2^{2r_{b_u}} - 1}}$ ,  $\theta = 2^{r_{b_u}} - 1$ ,  $\zeta_{b_u} = \theta - \frac{1}{2\vartheta_{b_u}\sqrt{\varpi_s}}$ ,  $\xi_{b_u} = \theta + \frac{1}{2\vartheta_{b_u}\sqrt{\varpi_s}}$ ,  $B_u$  is the complexity-accuracy trade-off parameter of the approximation, and  $\phi_n = \cos((2n-1)\pi/(2B_u))$ .

<sup>4</sup>Note that the analytical expressions for other important metrics such as outage probability, BLER, rate, etc., can be obtained simply by substituting the above-derived PDFs in the respective places and performing some mathematical simplifications.

$$f_{\gamma_u}(\gamma) \simeq \int_0^\infty x^{\frac{v-2}{4}} \frac{\exp\left(-\frac{a(x)^2}{2\sigma_{h_r}^2} - \frac{v(x)^2}{4q^2} - \frac{x+\lambda}{2}\right)}{4q\lambda^{\frac{v-2}{4}} \sqrt{2\pi\sigma_{h_r}^2} \gamma \alpha(x)} \left[ \Gamma\left(1, \frac{v(x)^2}{4q}\right) - \Gamma\left(1, q\left(\sqrt{\gamma\alpha(x)} - \frac{v(x)}{2q}\right)^2\right) \right. \\ \left. + \frac{v(x)}{2\sqrt{q}} \left( \Gamma\left(\frac{1}{2}, \frac{v(x)^2}{4q}\right) - \Gamma\left(\frac{1}{2}, q\left(\sqrt{\gamma\alpha(x)} - \frac{v(x)}{2q}\right)^2\right) \right) \right] I_{\frac{v}{2}-1}(\sqrt{\lambda x}) dx. \quad (25)$$

$$f_{\gamma_d}(\gamma) \simeq \frac{\exp\left(\frac{-p^2}{2\sigma_{g_r}^2} - \frac{w^2}{4t^2}\right)}{2t\sqrt{2\pi\sigma_{g_r}^2} \gamma \beta} \left[ \Gamma\left(1, \frac{w^2}{4t}\right) - \Gamma\left(1, t\left(\sqrt{\gamma\beta} - \frac{w}{2t}\right)^2\right) + \frac{w}{2\sqrt{t}} \left( \Gamma\left(\frac{1}{2}, \frac{w^2}{4t}\right) - \Gamma\left(\frac{1}{2}, t\left(\sqrt{\gamma\beta} - \frac{w}{2t}\right)^2\right) \right) \right]. \quad (27)$$

$$\varphi_{b_u} \simeq \vartheta_{b_u} \sqrt{\varpi_s} (\xi_{b_u} - \zeta_{b_u}) \sum_{n=1}^{B_u} \left( \frac{(\xi_{b_u} + \zeta_{b_u}) \pi \sqrt{1 - \phi_n^2} \exp\left(\frac{-a^2}{2\sigma_{h_r}^2} - \frac{v^2}{4q^2}\right)}{4qB_u \sqrt{\pi\sigma_{h_r}^2} (\xi_{b_u} + \zeta_{b_u}) \alpha} \right) \left[ -\Gamma\left(1, \frac{q}{2} \left( \sqrt{(\xi_{b_u} + \zeta_{b_u})(1 + \phi_n)\alpha} - \frac{v}{q} \right)^2 \right) \right. \\ \left. + \Gamma\left(1, \frac{v^2}{4q}\right) + \frac{v}{2\sqrt{q}} \left( \Gamma\left(\frac{1}{2}, \frac{v^2}{4q}\right) - \Gamma\left(\frac{1}{2}, \frac{q}{2} \left( \sqrt{(\xi_{b_u} + \zeta_{b_u})(1 + \phi_n)\alpha} - \frac{v}{q} \right)^2 \right) \right) \right]. \quad (33)$$

*Proof.* It is extremely difficult to compute  $\varphi_{b_u}$  from (32) in a closed-form expression due to the involvement of the  $Q$  function. Therefore, we utilise the piecewise-linear approximation of  $Q\left(\frac{C(\gamma_u) - r_{b_u}}{\sqrt{V(\gamma_u)/\varpi_s}}\right) \triangleq \Xi(\gamma_u)$  which is expressed as [49]

$$\Xi(\gamma_u) = \begin{cases} 1, & \gamma_u \leq \zeta_{b_u}, \\ 0.5 - \vartheta_{b_u} \sqrt{\varpi_s} (\gamma_u - \theta), & \zeta_{b_u} < \gamma_u < \xi_{b_u}, \\ 0, & \gamma_u \geq \xi_{b_u}. \end{cases} \quad (34)$$

The final BLER is determined by taking the mean of  $\Xi(\gamma_u)$  with respect to the PDF of  $\gamma_u$ , evaluated as

$$\varphi_{b_u} \approx \int_0^\infty \Xi(x) f_{\gamma_u}(x) dx, \quad (35)$$

where  $f_{\gamma_u}(x)$  is given in (7). Applying integration by parts to (35),  $\varphi_{b_u}$  can be simplified as

$$\varphi_{b_u} \approx \int_0^\infty \Xi(x) F_{\gamma_u}(x) \\ = [\Xi(x) F_{\gamma_u}(x)]_0^\infty - \int_0^\infty F_{\gamma_u}(x) d\Xi(x), \quad (36)$$

where  $F_{\gamma_u}(x)$  is the CDF of the SINR  $\gamma_u$ . Differentiating  $\Xi(x)$  in (34) with respect to  $x$  and substituting the result into (36), the BLER becomes

$$\varphi_{b_u} = \vartheta_{b_u} \sqrt{\varpi_s} \int_{\zeta_{b_u}}^{\xi_{b_u}} F_{\gamma_u}(x) dx. \quad (37)$$

Solving (37) using the Riemann integral approximation  $\int_a^b g(y) dy = (b-a)g((a+b)/2)$ , we have

$$\varphi_{b_u} \approx \vartheta_{b_u} \sqrt{\varpi_s} (\xi_{b_u} - \zeta_{b_u}) F_{\gamma_u}((\xi_{b_u} + \zeta_{b_u})/2). \quad (38)$$

In order to solve (38), we need to determine the CDF  $F_{\gamma_u}$ . Using the PDF  $f_{\gamma_u}$ , the CDF can be evaluated as

$$F_{\gamma_u}(\gamma) = \int_0^\gamma f_{\gamma_u}(x) dx. \quad (39)$$

Substituting  $f_{\gamma_u}$  from (7) into (39) and applying the Gaussian-Chebyshev quadrature (GCQ) method [46, 25.4.30], we have (40), which is given on top of the next page, where  $R_{B_u}$  denotes the error term. Note that  $R_{B_u}$  becomes negligible for higher values of  $B_u$  [25], [46], hence it will not be included in further equations. Substituting (40) into (38), the expression for uplink BLER is obtained in (33). ■

Similarly, using (21) and (24), the achievable uplink BLER using the MM method at the AP can be approximated by

$$\varphi_{b_u}^{\text{MM}} \approx \frac{\vartheta_{b_u} \sqrt{\varpi_s} (\xi_{b_u} - \zeta_{b_u})}{\Gamma(\kappa_{z_u})} \\ \times \gamma \left( \kappa_{z_u}, \frac{(\xi_{b_u} + \zeta_{b_u})(P_{SI} + \sigma^2)}{2P_u \nu_{z_u}} \right). \quad (41)$$

## 2) Goodput Analysis

The uplink goodput is defined as the number of information bits reliably delivered from the UCU to AP via the RIS in a specific time period. Thus, the network goodput for the UCU is evaluated as [50]

$$\mathcal{G}_u = (\varpi_s / \varpi_{\text{tot},s}) r_u (1 - \varphi_{up}) \\ = (1 - (\varpi_{\text{train},s} / \varpi_{\text{tot},s})) r_u (1 - \varphi_{up}), \quad (42)$$

where  $r_u$  denotes the target rate for the uplink,  $\varpi_{\text{train},s}$  denotes the number of channel uses for uplink channel estimation, and  $\varpi_{\text{tot},s}$  denotes the number of channel uses to communicate the short packet (i.e.,  $\varpi_{\text{tot},s} = \varpi_{\text{train},s} + \varpi_s$ ). Note that for the case of a short code blocklength  $\varpi_s$  and a high training

$$F_{\gamma_u}(\gamma) = \sum_{n=1}^{B_u} \left( \frac{\gamma \pi \sqrt{1 - \phi_n^2} \exp\left(\frac{-a^2}{2\sigma_{h_r}^2} - \frac{v^2}{4q^2}\right)}{2qB_u \sqrt{\pi\sigma_{h_r}^2} 2\gamma\alpha} \right) \left[ \Gamma\left(1, \frac{v^2}{4q}\right) - \Gamma\left(1, \frac{q}{2} \left(\sqrt{2\gamma(1 + \phi_n)\alpha} - \frac{v}{q}\right)^2\right) \right. \\ \left. + \frac{v}{2\sqrt{q}} \left( \Gamma\left(\frac{1}{2}, \frac{v^2}{4q}\right) - \Gamma\left(\frac{1}{2}, \frac{q}{2} \left(\sqrt{2\gamma(1 + \phi_n)\alpha} - \frac{v}{q}\right)^2\right) \right) \right] + R_{B_u}. \quad (40)$$

overhead  $\varpi_{\text{train},s}$  (corresponding to a large number of RIS elements), the goodput can be low due to a low value of the fraction  $\varpi_{\text{train},s}/\varpi_{\text{tot},s}$ , and therefore such use cases are to be avoided in practice. Some results illustrating the tradeoffs involved in achieving high goodput are provided in Section VII.

### 3) Downlink BLER

Let  $\varphi_{b_d}$  denote the downlink BLER of the considered RIS-assisted wireless network, assuming that the DCU transmits  $c_{dp}$  information bits in  $\varpi_d$  channel uses (i.e., the blocklength of the channel code is  $\varpi_d$ ). Thus the code rate (in bits per channel use) is given by  $r_{b_d} = c_{dp}/\varpi_d$ . Similar to the uplink case, we can write the BLER for downlink transmission as

$$\varphi_{b_d} \approx \mathbb{E} \left\{ Q \left( \frac{C(\gamma_d) - r_{b_d}}{\sqrt{V(\gamma_d)/\varpi_d}} \right) \right\}, \quad (43)$$

where  $C(\gamma_d) = \log_2(1 + \gamma_d)$  is the Shannon capacity and  $V(\gamma_d) = (1 - (1 + \gamma_d)^{-2}) (\log_2 e)^2$  is the channel dispersion.

**Theorem 2.** *The achievable downlink BLER at the DCU can be approximated by (44), which is given on top of the next page, where  $\mu_{g_r} = N \left( \frac{\Omega_3 \Omega_4}{m_3 m_4} \right)^{\frac{1}{2}} \frac{\Gamma(m_3 + 0.5) \Gamma(m_4 + 0.5)}{\Gamma(m_3) \Gamma(m_4)}$ ,  $\sigma_{g_r}^2 = N \Omega_3 \Omega_4 - \frac{\mu_{g_r}^2}{N}$ ,  $p = \gamma\beta - \mu_{g_r}$ ,  $t = \frac{1 + \sigma_{g_r}^2}{2\sigma_{g_r}^2}$ ,  $w = \frac{p}{\sigma_{g_r}^2}$ ,  $\beta = \frac{\sigma_{g_r}^2}{P_b}$ ,  $\vartheta_{b_d} = \frac{1}{2\pi \sqrt{2^{2r_{b_d}} - 1}}$ ,  $\theta_{b_d} = 2^{r_{b_d}} - 1$ ,  $\zeta_{b_d} = \theta_{b_d} - \frac{1}{2\vartheta_{b_d} \sqrt{\varpi_d}}$  and  $\xi_{b_d} = \theta_{b_d} + \frac{1}{2\vartheta_{b_d} \sqrt{\varpi_d}}$ ,  $B_d$  is the complexity-accuracy trade-off parameter, and  $\phi_n = \cos((2n - 1)\pi/(2B_d))$ .*

*Proof.* Similar to (34), we can approximate  $Q \left( \frac{C(\gamma_d) - r_{b_d}}{\sqrt{V(\gamma_d)/\varpi_d}} \right)$  as

$$\aleph(\gamma_d) = \begin{cases} 1, & \gamma_d \leq \zeta_{b_d}, \\ 0.5 - \vartheta_{b_d} \sqrt{\varpi_d} (\gamma_d - \theta_{b_d}), & \zeta_{b_d} < \gamma_d < \xi_{b_d}, \\ 0, & \gamma_d \geq \xi_{b_d}. \end{cases} \quad (45)$$

The BLER for downlink transmission is determined by taking the mean of  $\aleph(\gamma_d)$  with respect to the PDF of  $\gamma_d$  as

$$\varphi_{b_d} \approx \int_0^\infty \aleph(y) f_{\gamma_d}(y) dy, \quad (46)$$

where  $f_{\gamma_d}$  is given in (27). Applying integration by parts to (46),  $\varphi_{b_d}$  can be written as

$$\varphi_{b_d} \approx \vartheta_{b_d} \sqrt{\varpi_d} \int_{\zeta_{b_d}}^{\xi_{b_d}} F_{\gamma_d}(y) dy \\ = \vartheta_{b_d} \sqrt{\varpi_d} (\xi_{b_d} - \zeta_{b_d}) F_{\gamma_d} \left( \frac{\xi_{b_d} + \zeta_{b_d}}{2} \right), \quad (47)$$

where  $F_{\gamma_d}$  is the CDF of the SNR  $\gamma_d$ . Note that  $F_{\gamma_d}$  can be obtained using an approach similar to (40) and is given by (48), which is given on top of the next page, Substituting (48) into (47), the final expression for  $\varphi_{b_d}$  is obtained as (44). ■

Similarly, using (21) and (31), the achievable downlink BLER using the MM method at the DCU is given by

$$\varphi_{b_d}^{\text{MM}} \approx \frac{\vartheta_{b_d} \sqrt{\varpi_d} (\xi_{b_d} - \zeta_{b_d})}{\Gamma(\kappa_{z_d})} \gamma \left( \kappa_{z_d}, \left( \frac{(\xi_{b_d} + \zeta_{b_d}) \sigma^2}{2P_b \nu_{z_d}} \right) \right). \quad (49)$$

### 4) Goodput Analysis

The goodput is defined as the number of information bits reliably delivered from the AP to DCU via the RIS in a specific time period. The goodput for the DCU is evaluated as

$$G_d = (\varpi_d / \varpi_{\text{tot},d}) r_d (1 - \varphi_{dp}) \\ = (1 - (\varpi_{\text{train},d} / \varpi_{\text{tot},d})) r_d (1 - \varphi_{dp}), \quad (50)$$

where  $r_d$  denotes the target rate for the downlink,  $\varpi_{\text{train},d}$  denotes the number of channel uses for uplink channel estimation, and  $\varpi_{\text{tot},d}$  denotes the number of channel uses to communicate the short packet (i.e.,  $\varpi_{\text{tot},d} = \varpi_{\text{train},d} + \varpi_d$ ).

## B. Infinite Block-Length Analysis

### 1) Uplink Outage Probability

For the case of conventional (infinite blocklength) communication, the uplink outage probability is given by

$$P_{\text{Ou}} = \Pr(\gamma_u < \gamma_{th}^u), \quad (51)$$

where  $\gamma_{th}^u = 2^{r_u} - 1$  and the target uplink rate is  $r_u$ .

**Theorem 3.** *The uplink outage probability at the AP can be approximated by (52), which is given on top of the next page, where  $\mu_{h_r} = K \left( \frac{\Omega_1 \Omega_2}{m_1 m_2} \right)^{\frac{1}{2}} \frac{\Gamma(m_1 + 0.5) \Gamma(m_2 + 0.5)}{\Gamma(m_1) \Gamma(m_2)}$ ,*

*$\sigma_{h_r}^2 = \frac{K \Omega_1 \Omega_2}{K} - \frac{\mu_{h_r}^2}{K}$ ,  $a = \sqrt{\gamma_{th}^u \alpha} - \mu_{h_r}$ ,  $q = (1 + \sigma_{h_r}^2) / (2\sigma_{h_r}^2)$ ,  $v = a / \sigma_{h_r}^2$  and  $\alpha = (P_{SI} + \sigma^2) / P_u$ ,  $B_u$  is the complexity-accuracy trade-off parameter and  $\phi_n = \cos((2n - 1)\pi / (2B_u))$ .*

*Proof.* The right hand side of (51) can be expressed in terms of the CDF of  $\gamma_u$  as

$$\Pr(\gamma_u < \gamma_{th}^u) = F_{\gamma_u}(\gamma_{th}^u). \quad (53)$$

Substituting (40) into (53), we obtain (52). ■

Similarly, using (21) and (24), the uplink outage probability at the AP using the MM method can be approximated as

$$\begin{aligned} \varphi_{b_d} \simeq & \vartheta_{b_d} \sqrt{\varpi_d} (\xi_{b_d} - \zeta_{b_d}) \sum_{n=1}^{B_d} \left( \frac{(\xi_{b_d} + \zeta_{b_d}) \pi \sqrt{1 - \phi_n^2} \exp\left(\frac{-p^2}{2\sigma_{g_r}^2} - \frac{w^2}{4t^2}\right)}{4t B_d \sqrt{\pi \sigma_{g_r}^2} (\xi_{b_d} + \zeta_{b_d}) \beta} \right) \left[ -\Gamma\left(1, \frac{w}{2} \left(\sqrt{(\xi_{b_d} + \zeta_{b_d})(1 + \phi_n)\beta} - \frac{w}{t}\right)^2\right) \right. \\ & \left. + \Gamma\left(1, \frac{w^2}{4t}\right) + \frac{w}{2\sqrt{t}} \left( \Gamma\left(\frac{1}{2}, \frac{w^2}{4t}\right) - \Gamma\left(\frac{1}{2}, \frac{t}{2} \left(\sqrt{(\xi_{b_d} + \zeta_{b_d})(1 + \phi_n)\beta} - \frac{w}{t}\right)^2\right) \right) \right]. \end{aligned} \quad (44)$$

$$\begin{aligned} F_{\gamma_d}(\gamma) = & \sum_{n=1}^{B_d} \left( \frac{\gamma \pi \sqrt{1 - \phi_n^2} \exp\left(\frac{-p^2}{2\sigma_{g_r}^2} - \frac{w^2}{4t^2}\right)}{2t B_d \sqrt{\pi \sigma_{g_r}^2} 2\gamma \beta} \right) \left[ \Gamma\left(1, \frac{w^2}{4t}\right) - \Gamma\left(1, \frac{t}{2} \left(\sqrt{2\gamma(1 + \phi_n)\beta} - \frac{w}{t}\right)^2\right) \right. \\ & \left. + \frac{w}{2\sqrt{t}} \left( \Gamma\left(\frac{1}{2}, \frac{w^2}{4t}\right) - \Gamma\left(\frac{1}{2}, \frac{t}{2} \left(\sqrt{2\gamma(1 + \phi_n)\beta} - \frac{w}{t}\right)^2\right) \right) \right]. \end{aligned} \quad (48)$$

$$\begin{aligned} P_{O_u} = & \sum_{b_u=1}^{B_u} \left( \frac{\gamma_{th}^u \pi \sqrt{1 - \phi_{b_u}^2} \exp\left(\frac{-a^2}{2\sigma_{h_r}^2} - \frac{v^2}{4q^2}\right)}{4q B_u \sqrt{2\pi \sigma_{h_r}^2} \gamma_{th}^u \alpha} \right) \left[ \Gamma\left(1, \frac{v^2}{4q}\right) - \Gamma\left(1, \frac{q}{2} \left(\sqrt{2\gamma_{th}^u(1 + \phi_{b_u})\alpha} - \frac{v}{q}\right)^2\right) \right. \\ & \left. + \frac{v}{2\sqrt{q}} \left( \Gamma\left(\frac{1}{2}, \frac{v^2}{4q}\right) - \Gamma\left(\frac{1}{2}, \frac{q}{2} \left(\sqrt{2\gamma_{th}^u(1 + \phi_{b_u})\alpha} - \frac{v}{q}\right)^2\right) \right) \right]. \end{aligned} \quad (52)$$

$$P_{O_u}^{MM} \approx \frac{1}{\Gamma(\kappa_{z_u})} \gamma \left( \kappa_{z_u}, \frac{\gamma_{th}^u (P_{SI} + \sigma^2)}{P_u \nu_{z_u}} \right). \quad (54)$$

The throughput of the uplink communication at a target uplink rate  $r_u$  is defined by

$$T_u = (1 - P_{O_u}) r_u. \quad (55)$$

### 2) Downlink Outage Probability

For the case of conventional (infinite blocklength) communication, the downlink outage probability is given by

$$P_{O_d} = \Pr(\gamma_d < \gamma_{th}^d), \quad (56)$$

where  $\gamma_{th}^d = 2^{r_d} - 1$  and the target downlink rate is  $r_d$ .

**Theorem 4.** *The downlink outage probability at the DCU can be approximated by (57), which is given on top of the next page, where  $\mu_{g_r} = N \left( \frac{\Omega_3 \Omega_4}{m_3 m_4} \right)^{\frac{1}{2}} \frac{\Gamma(m_3 + 0.5) \Gamma(m_4 + 0.5)}{\Gamma(m_3) \Gamma(m_4)}$ ,  $\sigma_{g_r}^2 = N \Omega_3 \Omega_4 - \frac{\mu_{g_r}^2}{N}$ ,  $p = \sqrt{\gamma_{th}^d \beta} - \mu_{g_r}$ ,  $t = \frac{1 + \sigma_{g_r}^2}{2\sigma_{g_r}^2}$ ,  $w = \frac{p}{\sigma_{g_r}^2}$ , and  $\beta = \frac{\sigma^2}{P_b}$ ,  $B_d$  is the complexity-accuracy trade-off parameter and  $\phi_{b_d} = \cos\left(\frac{(2b_d - 1)\pi}{2B_d}\right)$ .*

*Proof.* The right hand side of (56) can be expressed in terms of the CDF of  $\gamma_d$  as

$$\Pr(\gamma_d < \gamma_{th}^d) = F_{\gamma_d}(\gamma_{th}^d). \quad (58)$$

Substituting (48) into (58), we obtain (57). ■

Similarly, using (21) and (31), the downlink outage probability at the DCU using the MM method can be approximated as

$$P_{O_d}^{MM} \approx \frac{1}{\Gamma(\kappa_{z_d})} \gamma \left( \kappa_{z_d}, \frac{\gamma_{th}^d \sigma^2}{P_b \nu_{z_d}} \right). \quad (59)$$

The throughput of the downlink communication at a target downlink rate  $r_d$  is defined by

$$T_d = (1 - P_{O_d}) r_d. \quad (60)$$

### 3) Case where AP acts as an FD relay

Note that, in this work, the AP is acting as a base station which is receiving data symbols from the uplink user and simultaneously transferring other data symbols to the downlink user. It is noteworthy that the analysis presented in this work can also be used for an FD relay network. In particular, using (4) and (6), the end-to-end SINR with the AP acting as an FD relay can be expressed as

$$\gamma_{e2e} = \min\{\gamma_u, \gamma_d\}. \quad (61)$$

Further, the outage probability of the relay network can be evaluated as

$$P_O = \Pr(\gamma_{e2e} \leq \gamma_{th}^d) = \Pr(\min\{\gamma_u, \gamma_d\} \leq \gamma_{th}^d).$$

Using  $P_{O_u}$  and  $P_{O_d}$  from (52) and (57), respectively, we obtain

$$P_O = P_{O_u} + P_{O_d} - P_{O_u} P_{O_d}.$$

$$\begin{aligned}
P_{\text{Od}} = & \sum_{b_d=1}^{B_d} \left( \frac{\gamma_{th}^d \pi \sqrt{1 - \phi_{b_d}^2} \exp\left(\frac{-p^2}{2\sigma_{gr}^2} - \frac{w^2}{4t^2}\right)}{4t B_d \sqrt{2\pi\sigma_{gr}^2} \gamma_{th}^d \beta} \right) \left[ \Gamma\left(1, \frac{w^2}{4t}\right) - \Gamma\left(1, \frac{t}{2} \left(\sqrt{2\gamma_{th}^d(1 + \phi_{b_d})\beta} - \frac{w}{t}\right)^2\right) \right. \\
& \left. + \frac{w}{2\sqrt{t}} \left( \Gamma\left(\frac{1}{2}, \frac{w^2}{4t}\right) - \Gamma\left(\frac{1}{2}, \frac{t}{2} \left(\sqrt{2\gamma_{th}^d(1 + \phi_{b_d})\beta} - \frac{w}{t}\right)^2\right) \right) \right]. \quad (57)
\end{aligned}$$

## V. RATE ANALYSIS

### A. Uplink Rate Analysis

The maximum achievable rate in the uplink FBL transmission can be tightly approximated as

$$R_{up} \approx C(\gamma_u) - \sqrt{V(\gamma_u)/\varpi_s} Q^{-1}(\tilde{\varphi}_{b_u}), \quad (62)$$

where  $C(\gamma_u) = \log_2(1 + \gamma_u)$  is the Shannon capacity,  $V(\gamma_u) = (1 - (1 + \gamma_u)^{-2})$  is the channel dispersion,  $\tilde{\varphi}_{b_u}$  is the constant desired BLER for uplink transmission and  $Q^{-1}(\cdot)$  is the inverse Q-function. Therefore, (62) can be written as

$$\begin{aligned}
R_{up} = & \log_2(1 + \gamma_u) \\
& - Q^{-1}(\tilde{\varphi}_{b_u}) \log_2 e \sqrt{1 - (1 + \gamma_u)^{-2}} / \sqrt{\varpi_s}. \quad (63)
\end{aligned}$$

The average rate can be expressed as  $\mathbb{E}[R_{up}]$ .

**Theorem 5.** *The maximum achievable rate in uplink FBL transmission is tightly approximated as*

$$\begin{aligned}
\tilde{R}_{up} \approx & \sum_{i=1}^{\mathcal{D}} \left( \frac{w_i}{(1 + t_b)} - \frac{Q^{-1}(\tilde{\varphi}_{b_u}) w_i}{\sqrt{\varpi_s} (1 + t_b)^2 \sqrt{t_b^2 + 2t_b}} \right) \\
& \times (\exp(t_b) (1 - F_{\gamma_u}(t_b))), \quad (64)
\end{aligned}$$

where  $F_{\gamma_u}(t_b)$  can be obtained by substituting  $(\gamma = t_b)$  in (40).  $\mathcal{D}$  denotes the accuracy-complexity trade-off factor,  $t_b$  represents  $i^{\text{th}}$  root of the generalized Laguerre polynomial  $L_{\mathcal{D}}(\cdot)$ , and  $w_i = \frac{t_b}{(m+1)^2 [L_{m+1}(t_b)]^2}$ .

*Proof.* Solving  $\mathbb{E}[R_{up}]$  with respect to PDF of  $\gamma_u$ , we get

$$\begin{aligned}
\mathbb{E}[R_{up}] \approx & \int_0^{\infty} \left( \frac{1}{1+x} - \frac{Q^{-1}(\tilde{\varphi}_{b_u}) \log_2 e}{\sqrt{\varpi_s} (1+x)^2 (\sqrt{x^2 + 2x})} \right) \\
& \times (1 - F_{\gamma_u}(x)) dx, \quad (65)
\end{aligned}$$

Substituting the expression for  $F_{\gamma_u}$  into (65) and solve using the Gaussian-Laguerre quadrature method [43], we obtain (64). ■

**Corollary 1.** *When  $\varpi_s \rightarrow \infty$ , the maximum achievable rate can be obtained using (64) as*

$$\tilde{R}_{UL} \approx \sum_{i=1}^{\mathcal{D}} w_i \exp(t_b) (1 - F_{\gamma_u}(t_b)) / (1 + t_b). \quad (66)$$

### B. Downlink Rate Analysis

The maximum achievable rate in downlink FBL transmission can be tightly approximated as

$$R_{dl} \approx C(\gamma_d) - \sqrt{V(\gamma_d)/\varpi_d} Q^{-1}(\tilde{\varphi}_{b_d}), \quad (67)$$

(67) can be written as

$$\begin{aligned}
R_{dl} = & \log_2(1 + \gamma_d) \\
& - Q^{-1}(\tilde{\varphi}_{b_d}) \log_2 e \sqrt{1 - (1 + \gamma_d)^{-2}} / \varpi_d. \quad (68)
\end{aligned}$$

The average rate can be expressed as  $\tilde{R}_{dl} = \mathbb{E}[R_{dl}]$ .

**Theorem 6.** *The maximum achievable rate in downlink FBL transmission is given by*

$$\begin{aligned}
\tilde{R}_{dl} \approx & \sum_{n=1}^{\mathcal{M}} \left( \frac{w_n}{(1 + t_n)} - \frac{Q^{-1}(\tilde{\varphi}_{b_d}) w_n}{\sqrt{\varpi_d} (1 + t_n)^2 \sqrt{t_n^2 + 2t_n}} \right) \\
& \times (\exp(t_n) (1 - F_{\gamma_d}(t_n))), \quad (69)
\end{aligned}$$

where  $F_{\gamma_d}(t_n)$  can be obtained by substituting  $(\gamma = t_n)$  in (48).  $\mathcal{M}$  denotes the respective accuracy-complexity trade-off factor;  $t_n$  represents the  $n^{\text{th}}$  root of the generalized Laguerre polynomial  $L_{\mathcal{M}}(\cdot)$ , and  $w_n = t_n / ((n+1)^2 [L_{n+1}(t_n)]^2)$ .

*Proof.*  $\tilde{R}_{dl} = \mathbb{E}[R_{dl}]$  is solved following steps similar to (65). ■

**Corollary 2.** *The downlink rate when  $\varpi_d \rightarrow \infty$  can be obtained from (69) as*

$$\tilde{R}_{DN} \approx \sum_{n=1}^{\mathcal{M}} w_n \exp(t_n) (1 - F_{\gamma_d}(t_n)) / (1 + t_n). \quad (70)$$

## VI. EXTENSION TO MULTI-USER SCENARIO

In this section, the generalization of the considered setup to the more practical case with multiple users is discussed. Although the analysis remains the same when analyzing the channel gain for the downlink transmission, there will be significant differences when multiple UCUs are considered because of the different channel gain of the UCU-RIS- $R_u$  link and UCU-AP link.

We first investigate the downlink transmission where the AP uses NOMA [31] to form a superimposed data symbol for  $L$  DCUs given by

$$s_d = \sqrt{\eta_1 P_b} s_{d1} + \cdots + \sqrt{\eta_l P_b} s_{dl} + \cdots + \sqrt{\eta_L P_b} s_{dL}, \quad (71)$$

where  $\eta_l$  is the power allocation factor for the symbol  $s_{dl}$  intended for the  $l^{\text{th}}$  DCU. Thus, the signal received at the  $l^{\text{th}}$  DCU is given by

$$y_{dl} = (g_{bdl} + \mathbf{g}_{dl} \Phi \mathbf{g}_b) s_d + n_d, \quad (72)$$

where  $\mathbf{g}_{dl} = [g_{1dl}, g_{2dl}, \dots, g_{Ndl}]$ ,  $\mathbf{g}_b = [g_{b1}, g_{b2}, \dots, g_{bN}]^H$  and  $n_d \sim \mathcal{CN}(0, \sigma^2)$ . Without loss of generality, it is assumed that  $||g_{bd1} + \mathbf{g}_{d1} \Phi \mathbf{g}_b|| < |g_{bd2} + \mathbf{g}_{d2} \Phi \mathbf{g}_b| \cdots < |g_{bdL} +$

$\mathbf{g}_{dl}\Phi\mathbf{g}_b$ ] [28]. According to the NOMA principle, the  $l^{th}$  DCU needs to decode the signal  $s_{di}\forall i \in \{1, 2, \dots, l-1\}$  from  $y_{dl}$ , with an SINR of

$$\gamma_{dl,i} = \frac{|g_{bdl} + \mathbf{g}_{dl}\Phi\mathbf{g}_b|^2 \eta_i P_b}{\sum_{j=i+1}^L |g_{bdl} + \mathbf{g}_{dl}\Phi\mathbf{g}_b|^2 \eta_j P_b + \sigma^2}. \quad (73)$$

After decoding each symbol, SIC is performed to remove that symbol from the received signal. After  $l-1$  iterations of SIC, the  $l^{th}$  user decodes its own signal  $s_{dl}$  with an SINR of

$$\gamma_{dl} = \frac{|g_{bdl} + \mathbf{g}_{dl}\Phi\mathbf{g}_b|^2 \eta_l P_b}{\sum_{j=l+1}^L |g_{bdl} + \mathbf{g}_{dl}\Phi\mathbf{g}_b|^2 \eta_j P_b + \sigma^2}. \quad (74)$$

Let  $Z_{dl} = |g_{bdl} + \mathbf{g}_{dl}\Phi\mathbf{g}_b|$ . Note that the PDF of  $Z_{dl}^2$  can be derived similarly to (16). Next, due to the multi-step SIC, the outage probability at the  $l^{th}$  DCU can be expressed as

$$P_{Odl} = 1 - \Pr(\gamma_{dl,i} \geq \gamma_{di}^{th} \forall i \in \{1, 2, \dots, l-1\}, \gamma_{dl} \geq \gamma_{dl}^{th}), \quad (75)$$

where  $\gamma_{di}^{th} = 2^{R_{di}} - 1 \forall i \in \{1, 2, \dots, l\}$  is the minimum required SINR threshold corresponding to the target rate  $R_{di}$  of the  $i^{th}$  DCU.

**Theorem 7.** *The outage probability at the  $l^{th}$  DCU can be approximated as (76), which is given on top of the next page, where  $\mu_{g_{rl}} = N \left( \frac{\Omega_3 \Omega_{4l}}{m_3 m_{4l}} \right)^{\frac{1}{2}} \frac{\Gamma(m_3 + 0.5) \Gamma(m_{4l} + 0.5)}{\Gamma(m_3) \Gamma(m_{4l})}$ ,  $\sigma_{g_{rl}}^2 = N \Omega_3 \Omega_{4l} - \frac{\mu_{g_{rl}}^2}{N}$ ,  $p = \sqrt{z} - \mu_{g_{rl}}$ ,  $t = \frac{1 + \sigma_{g_{rl}}^2}{2\sigma_{g_{rl}}^2}$ ,  $w = p/\sigma_{g_{rl}}^2$ .  $m_3$  and  $\Omega_3$  are the shape and spread parameter of  $g_{bn}$ ,  $\forall n \in \mathcal{N}$ ,  $m_{4l}$  and  $\Omega_{4l}$  are the shape and spread parameter of  $g_{ndl}$ ,  $\forall n \in \mathcal{N}$ ,  $\hat{\gamma}_{dl}^{th} = \max(\hat{\gamma}_{dl}^{th}, \hat{\gamma}_{li}^{th} \forall i \in \{1, 2, \dots, l-1\})$ ,  $\hat{\gamma}_{dl}^{th} = \frac{\gamma_{dl}^{th} \sigma^2}{\eta_l P_b - \sum_{j=l+1}^L \eta_j P_b \gamma_{dl}^{th}}$ ,  $\hat{\gamma}_{li}^{th} = \frac{\gamma_{di}^{th} \sigma^2}{\eta_i P_b - \sum_{j=i+1}^L \eta_j P_b \gamma_{di}^{th}}$ .*

*Proof.* Substituting (73) and (74) into (75) and performing some simplification, we obtain

$$P_{Odl} = \Pr(|\mathbf{g}_{dl}\Phi\mathbf{g}_b + g_{bdl}|^2 \leq \hat{\gamma}_{dl}^{th}). \quad (77)$$

Solving (77) using steps similar to (57), we obtain (76). ■

Note that the optimum phase shift matrix can be found by following standard optimization tools [51], thus details are omitted due to space limitations. Next,  $\varphi_{dl}^{(i)}$  and  $\varphi_{dl}^{(l)}$  represents the BLER at the  $l^{th}$  user corresponding to (73) and (74), respectively.

Next, the closed-form expression of  $\varphi_{dl}^{(i)}$  can be obtained by substituting  $\gamma_{dl,i}$ ,  $r_{b_{dl}}$  and  $\varpi_{dl}$  in place of  $\gamma_d$ ,  $r_{b_d}$  and  $\varpi_d$ , respectively, in (43), and thereafter using an approach similar to that of (44). The achievable average downlink BLER at the  $l^{th}$  DCU can be expressed as

$$\varphi_{dl} = \varphi_{dl}^{(1)} + \left(1 - \varphi_{dl}^{(1)}\right) \varphi_{dl}^{(2)} + \dots + \left(1 - \varphi_{dl}^{(1)}\right) \left(1 - \varphi_{dl}^{(2)}\right) \dots \left(1 - \varphi_{dl}^{(l-1)}\right) \varphi_{dl}^{(l)}. \quad (78)$$

Similarly, for uplink transmission with  $M$  UCUs, the signal received at the AP is given by

$$y_u = \underbrace{\sum_{m=1}^M (h_{ubm} + \mathbf{h}_{um} \Theta \mathbf{h}_b)}_{\text{Signal received at the AP}} \sqrt{P_{um}} s_{um} + \underbrace{g_{bb} \sqrt{P_b} s_d}_{\text{SI}} + \underbrace{n_b}_{\text{AWGN}}, \quad (79)$$

where  $\mathbf{h}_b = [h_{1b}, h_{2b}, \dots, h_{Kb}]$ ,  $\mathbf{h}_{um} = [h_{um1}, h_{um2}, \dots, h_{umK}]^H$  and  $n_b \sim \mathcal{CN}(0, \sigma^2)$  is the AWGN,  $P_{um}$  denotes the transmit power used for transmitting the symbol  $s_{um}$  at the  $m^{th}$  UCU. Similar to downlink, we assume  $|h_{ubi} + \mathbf{h}_{ui} \Theta \mathbf{h}_b|^2 P_{ui} > |h_{ubj} + \mathbf{h}_{uj} \Theta \mathbf{h}_b|^2 P_{uj} \forall i > j$  where  $i, j \in \{1, 2, \dots, M\}$ . Thus, according to the NOMA principle, the AP will first decode the  $i^{th}$  UCU symbol, then perform SIC and decode the  $j^{th}$  UCU symbol. Therefore, the SINR for decoding  $s_m$  from  $y_u$  is given by

$$\gamma_{um} = \frac{|\mathbf{h}_{um} \Theta \mathbf{h}_b + h_{dm}|^2 P_{um}}{\sum_{j=m+1}^M |\mathbf{h}_{uj} \Theta \mathbf{h}_b + h_{dj}|^2 P_{uj} + P_{SI} + \sigma^2}. \quad (80)$$

Due to NOMA, the outage probability for the uplink transmission corresponding to the  $m^{th}$  UCU can be evaluated as

$$P_{Oum} = \Pr(\gamma_{ui} \leq \gamma_{ui}^{th} \forall i \in \{1, 2, \dots, m\}), \quad (81)$$

where  $\gamma_{um}^{th} = 2^{R_{um}} - 1 \forall m \in \{1, 2, \dots, M\}$  is the minimum required SINR threshold corresponding to the target rate  $R_{um}$  of the  $m^{th}$  UCU. Substituting  $\gamma_{um}$  from (80) into (81), we have

$$P_{Oum} = \Pr\left(\frac{|\mathbf{h}_{ui} \Theta \mathbf{h}_b + h_{di}|^2 P_{ui}}{\sum_{j=i+1}^M |\mathbf{h}_{uj} \Theta \mathbf{h}_b + h_{dj}|^2 P_{uj} + P_{SI} + \sigma^2} \leq \gamma_{ui}^{th}\right). \quad (82)$$

Note that the presence of  $\mathbf{h}_b$  in both the numerator and denominator of (82) leads to an intractable integration. However, with an aim to obtain useful insights, we resort to the earlier discussed MM method for  $M = 2$  and obtain an approximate closed-form<sup>5</sup> expression for the outage probability at each UCU in the following theorem.

**Theorem 8.** *The approximate outage probability at the AP for decoding the symbol corresponding to the first UCU can be evaluated as*

$$P_{Oul}^{MM} \approx I\left(\frac{\gamma_{u1}^{th} \hat{\nu}_{u2}}{\hat{\nu}_{u1} + \gamma_{u1}^{th} \hat{\nu}_{u2}}; \hat{\kappa}_{u1}, \hat{\kappa}_{u2}\right), \quad (83)$$

and the approximate outage probability for decoding the symbol corresponding to the second UCU is given by

$$P_{Oul}^{MM} \approx I\left(\frac{\gamma_{u1}^{th} \hat{\nu}_{u2}}{\hat{\nu}_{u1} + \gamma_{u1}^{th} \hat{\nu}_{u2}}; \hat{\kappa}_{u1}, \hat{\kappa}_{u2}\right) + \frac{\gamma\left(\kappa_{u2}, \frac{\gamma_{u2}^{th} (P_{SI} + \sigma^2)}{P_u \nu_{u2}}\right)}{\Gamma(\kappa_{u2})} \times \left(1 - I\left(\frac{\gamma_{u1}^{th} \hat{\nu}_{u2}}{\hat{\nu}_{u1} + \gamma_{u1}^{th} \hat{\nu}_{u2}}; \hat{\kappa}_{u1}, \hat{\kappa}_{u2}\right)\right), \quad (84)$$

<sup>5</sup>For simplicity, we consider  $M = 2$ . However, using the same method, the analytical expressions for more than two UCUs can be derived.

$$\begin{aligned}
P_{\text{Odl}} = & \sum_{b_d=1}^{B_d} \left( \frac{\tilde{\gamma}_{dl}^{th} \pi \sqrt{1 - \phi_{b_d}^2} \exp\left(\frac{-p^2}{2\sigma_{g_r}^2} - \frac{w^2}{4t^2}\right)}{4tB_d \sqrt{2\pi\sigma_{g_r}^2 \tilde{\gamma}_{dl}^{th}}} \right) \left[ \Gamma\left(1, \frac{w^2}{4t}\right) - \Gamma\left(1, \frac{t}{2} \left(\sqrt{2\tilde{\gamma}_{dl}^{th}(1 + \phi_{b_d})} - \frac{w}{t}\right)^2\right) \right] \\
& + \frac{w}{2\sqrt{t}} \left( \Gamma\left(\frac{1}{2}, \frac{w^2}{4t}\right) - \Gamma\left(\frac{1}{2}, \frac{t}{2} \left(\sqrt{2\tilde{\gamma}_{dl}^{th}(1 + \phi_{b_d})} - \frac{w}{t}\right)^2\right) \right). \quad (76)
\end{aligned}$$

TABLE I: Simulation Parameters

Para.	Value	Para.	Value	Para.	Value	Para.	Value
$\sigma^2$	-100 dBm	$P_{SI}$	-10 dBm	$r_u = r_d$	1	$a_{sp}$	50
$m_1$	2	$m_2$	2	$m_3$	2	$m_4$	2
$\Omega_1$	1	$\Omega_2$	1	$\Omega_3$	1	$\Omega_4$	1
AP - DCU	60m	UCU - $R_u$	3m	$\varpi_s(\varpi_d)$	150(200)	$c_{dp}$	70
$R_u$ - AP	50m	UCU - AP	50m	AP - $R_d$	60m	$R_d$ - DCU	5m

where  $I(\cdot; \cdot, \cdot)$  is the regularized incomplete beta function,

$$\begin{aligned}
\hat{\kappa}_{u2} &= \frac{(\kappa_{u2} P_{u2} \nu_{u2} + P_{SI} + \sigma^2)^2}{\kappa_{u2} (P_{u2} \nu_{u2})^2}, \quad \hat{\kappa}_{u1} = \kappa_{u1}, \quad \hat{\nu}_{u1} = P_{u1} \nu_{u1}, \\
\hat{\nu}_{u2} &= \frac{\kappa_{u2} (P_{u2} \nu_{u2})^2}{\kappa_{u2} P_{u2} \nu_{u2} + P_{SI} + \sigma^2}, \quad \kappa_{ui}, \nu_{ui} \text{ and other parameters for the } i^{\text{th}} \text{ DCU are obtained using the concept explained in Section II-B.}
\end{aligned}$$

*Proof.* For  $m = 1$  and  $M = 2$ , we rewrite (82) as

$$\begin{aligned}
P_{\text{Oul}} &= \Pr(\gamma_{u1} \leq \gamma_{u1}^{th}) \\
&= \Pr\left(\frac{Z_{u1}^2 P_{u1}}{Z_{u2}^2 P_{u2} + P_{SI} + \sigma^2} \leq \gamma_{u1}^{th}\right), \quad (85)
\end{aligned}$$

where  $Z_{ui} = |\mathbf{h}_{u_i} \mathbf{\Theta} \mathbf{h}_b + h_{di}|$  for  $i \in \{1, 2\}$ . We then assume that, similar to [44],  $Z_{u1}$  and  $Z_{u2}$  are approximately independent of each other. Thereafter, similar to (23), the distribution of  $Z_{u1}^2$  is approximated as  $\mathbb{G}(\kappa_{u1}, \nu_{u1})$ . Similarly,  $Z_{u2}^2$  follows the distribution  $\mathbb{G}(\psi_2, \nu_{u2})$ . From the aforementioned discussion, it can be noted that the SINR  $\gamma_{u1}$  equivalently can be represented as the ratio of two Gamma RVs and follows the beta prime distribution [45]. Thus, the CDF of  $\gamma_{u1}$  can be evaluated as

$$\Pr\{\gamma_{u1} \leq y\} = I\left(\frac{y \hat{\nu}_{u2}}{\hat{\nu}_{u1} + y \hat{\nu}_{u2}}; \hat{\kappa}_{u1}, \hat{\kappa}_{u2}\right). \quad (86)$$

Substituting  $y = \gamma_{u1}^{th}$  in (86), we obtain (83). Similarly, for  $m = 2$  and  $M = 2$ , we have

$$P_{\text{Oul}} = \Pr\left(\frac{Z_{u1}^2 P_{u1}}{Z_{u2}^2 P_{u2} + P_{SI} + 1} \leq \gamma_{u1}^{th}, \frac{Z_{u2}^2 P_{u2}}{P_{SI} + 1} \leq \gamma_{u2}^{th}\right). \quad (87)$$

Alternatively,  $P_{\text{Oul}}$  can be evaluated as

$$\begin{aligned}
P_{\text{Oul}} &= \Pr\left(\frac{Z_{u1}^2 P_{u1}}{Z_{u2}^2 P_{u2} + P_{SI} + 1} \leq \gamma_{u1}^{th}\right) \\
&+ \Pr\left(\frac{Z_{u1}^2 P_{u1}}{Z_{u2}^2 P_{u2} + P_{SI} + 1} > \gamma_{u1}^{th}\right) \Pr\left(\frac{Z_{u2}^2 P_{u2}}{P_{SI} + 1} \leq \gamma_{u2}^{th}\right). \quad (88)
\end{aligned}$$

Solving (88) using (21), we obtain (84). ■

Moreover, similar to (44), the average uplink BLER using the MM method at the AP can be approximated as

$$\varphi_2 \approx \varphi_{b_u} + (1 - \varphi_{b_u}) \hat{\varphi}_2, \quad (89)$$

where

$$\begin{aligned}
\varphi_{u1} &\approx \vartheta_{b_{u1}} \sqrt{\varpi_{u1}} (\xi_{b_{u1}} - \zeta_{b_{u1}}) \\
&\times I\left(\frac{(\xi_{b_{u1}} + \zeta_{b_{u1}}) \hat{\nu}_{u2}}{2\hat{\nu}_{u1} + (\xi_{b_{u1}} + \zeta_{b_{u1}}) \hat{\nu}_{u2}}; \hat{\kappa}_{u1}, \hat{\kappa}_{u2}\right),
\end{aligned}$$

and

$$\begin{aligned}
\varphi_{u2} &\approx \frac{\vartheta_{b_{u2}} \sqrt{\varpi_{u2}} (\xi_{b_{u2}} - \zeta_{b_{u2}})}{\Gamma(\kappa_{u2})} \\
&\times \gamma(\kappa_{u2}, (\xi_{b_{u2}} + \zeta_{b_{u2}})(P_{SI} + \sigma^2)/(2P_{u2}\nu_{u2})),
\end{aligned}$$

where  $\vartheta_{b_{ui}}, \varpi_{ui}, \xi_{b_{ui}}$  and  $\zeta_{b_{ui}}$  are the parameter for the  $i^{\text{th}}$  UCU described in Section IV-A.1.

## VII. RESULTS AND DISCUSSION

In this section, results demonstrating the performance of the RIS-assisted system and the effectiveness of the RISs are presented for FBL and IBL transmission. We also validate the accuracy of the derived analytical expressions using Monte-Carlo simulation represented by markers in the respective graphs. Table I contains the considered simulation parameters. Note that for simulations, we have considered the distance-dependent pathloss given by  $\zeta/D_i^{\tau_i}$  where  $\zeta$  is the reference pathloss with  $\zeta = -30\text{dB}$  for every link,  $D_i$  is used to denote the distance between transmitter and receiver nodes of the  $i^{\text{th}}$  link, and  $\tau_i$  is the pathloss exponent having a value of 3.8 for the direct paths (i.e. UCU-AP and AP-DCU) and 2.5 for RIS-aided links (i.e., UCU- $R_u$ ,  $R_u$ -AP, AP- $R_d$ , and  $R_u$ -DCU) [52]. Additionally, in order to have a better understanding of the impact of the RISs on the system performance, results are obtained considering three different cases: 1) ‘‘Direct-only/no-RIS/without-RIS link’’, 2) ‘‘RIS-only’’, and 3) ‘‘Direct+RIS’’.

### A. Results for FBL transmission

#### 1) Uplink Communication

Fig. 4 shows the variation of the average achievable BLER at the AP during uplink transmission ( $\varphi_{b_u}$ ) against the transmit power available at UCU ( $P_u$ ) for all three cases with FBL transmission, for different values of the number of elements at  $R_u(K)$ . The close proximity of the simulated BLER to  $\varphi_{b_u}$  derived in (33) validates its accuracy. It can be observed

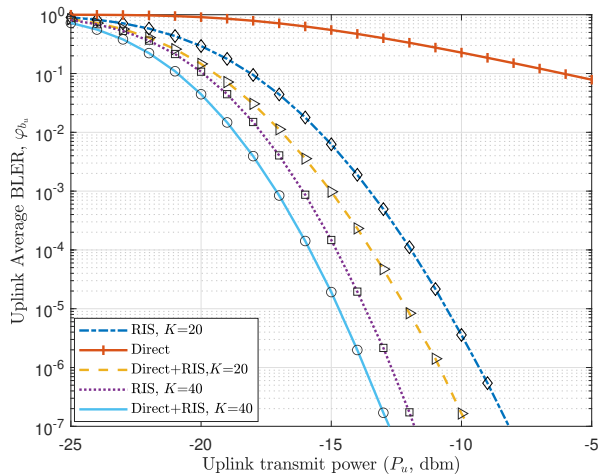


Fig. 4: Average BLER at AP vs uplink power.

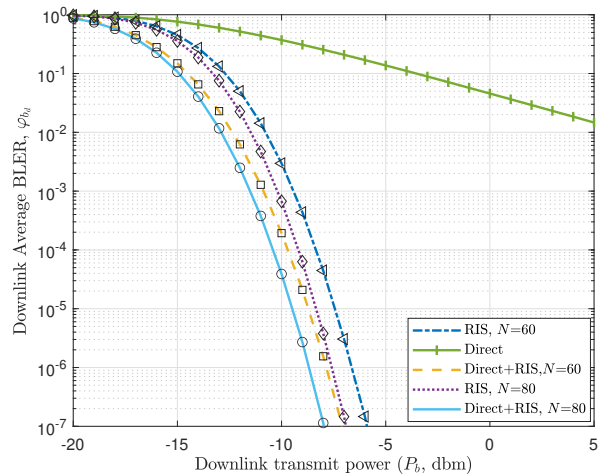


Fig. 6: Average BLER at AP vs downlink power.

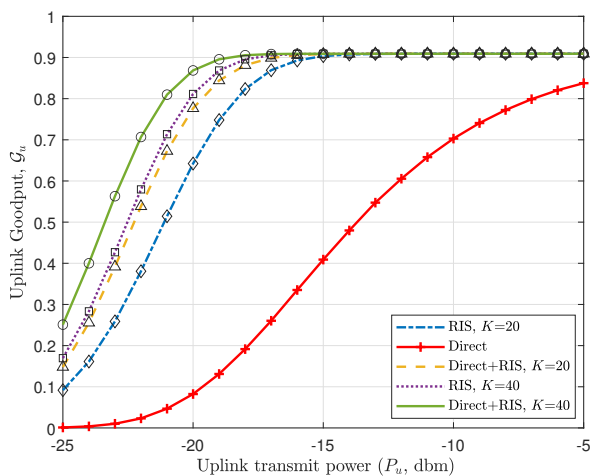


Fig. 5: Goodput at AP vs uplink power.

that the BLER improves with an increase in transmit power. All three cases provide similar performances at low power. However, at higher values of  $P_u$ , the Direct-only case has the worst performance among the three cases due to excessive fading and pathloss. The RIS-only case provides much better performance as compared to the Direct-only case due to the passive reflection from its elements. It clearly indicates that in the absence of the direct link between transmitter and receiver, the RIS can provide more diversity gain for information transfer. In addition to this, one can also observe a significant improvement in  $\varphi_{b_u}$  with an increase in  $K$ . Thus, one can always have an additional degree of freedom to achieve the desired QoS by increasing the number of elements at the RIS. Further, it can be seen that the best performance is obtained for the third case. It indicates that the use of RIS further enhances the achievable BLER when used with considerable direct path gain.

Fig. 5 depicts the achievable goodput ( $\mathcal{G}_u$ ) in uplink communication for all three cases considering FBL transmission by plotting  $\mathcal{G}_u$  against  $P_u$  for different values of  $K$ . It can

be observed that at low transmit power, the goodput of the system is very low for all three cases. However,  $\mathcal{G}_u$  in each case increases with an increase in  $P_u$ . It can be observed that, similar to the case of BLER, the Direct+RIS case provides the best goodput among all three cases. Further, one can also observe a significant increase in  $\mathcal{G}_u$  with an increase in  $K$  for the RIS-only and Direct+RIS cases. It can be seen that  $\mathcal{G}_u$  for the RIS-only and Direct+RIS cases saturates after a certain value of power. This is because of the fulfilment of the target rate at higher power in these two cases. However, due to better performance,  $\mathcal{G}_u$  in the Direct+RIS mode saturates earlier than the RIS-only mode.

## 2) Downlink Communication

Fig. 6 depicts the variation of the average achievable BLER at the DCU during downlink transmission ( $\varphi_{b_d}$ ) against the transmit power available at the AP ( $P_b$ ) for all three cases with FBL transmission, for different values of the number of RIS elements at  $R_d(N)$ . It can be observed that the average achievable BLER improves as the transmit power at the AP increases. The simulation results are in close agreement with the BLER expression derived in (44), which demonstrates the accuracy of the derived analytical expression. As evident from the figure, there is a notable improvement in the average BLER for the RIS-only and Direct+RIS cases due to a considerable channel gain with increasing  $N$ . Similar to uplink communication, the Direct+RIS case in downlink communication provides lower BLER throughout the range of  $P_b$ . This indicates that the use of RIS can provide a significant improvement in the achievable BLER for downlink communication.

Fig. 7 presents the achievable goodput ( $\mathcal{G}_d$ ) in downlink communication for all three cases considering FBL transmission by plotting  $\mathcal{G}_d$  against  $P_b$  for different values of  $N$ . At low transmit power, the goodput of the system is very poor for all three cases. Also, with an increase in  $P_b$ ,  $\mathcal{G}_d$  also increases. However, due to the fulfillment of the target rate,  $\mathcal{G}_d$  for each user saturates after a certain value of power. For example, when  $N = 80$ , the Direct+RIS and RIS-only cases achieve the target rate of unity at  $P_b = -13$  dBm and  $P_b = -10$

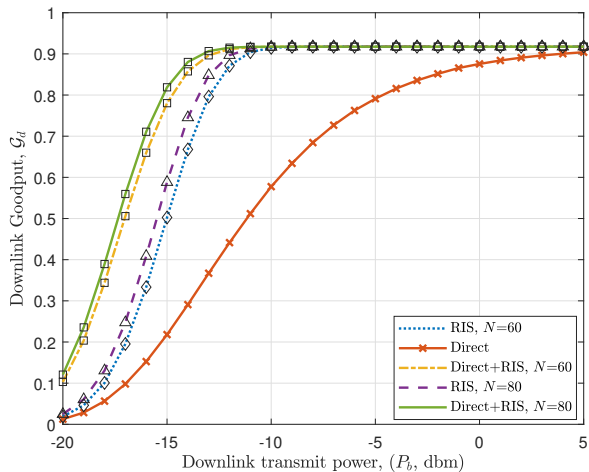


Fig. 7: Goodput at DCU vs downlink power.

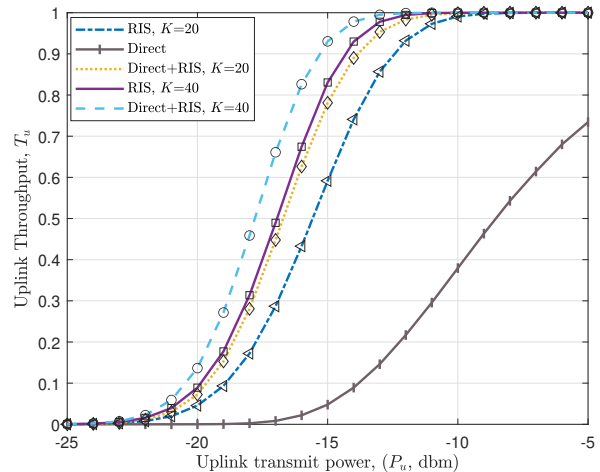


Fig. 9: Throughput at AP vs uplink power.

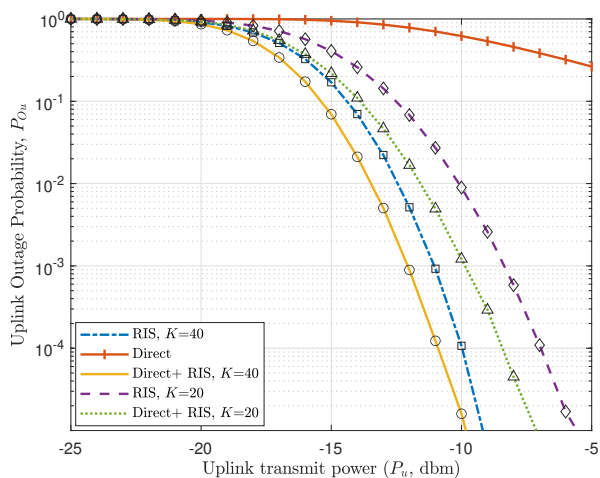


Fig. 8: Outage probability at AP vs uplink power.

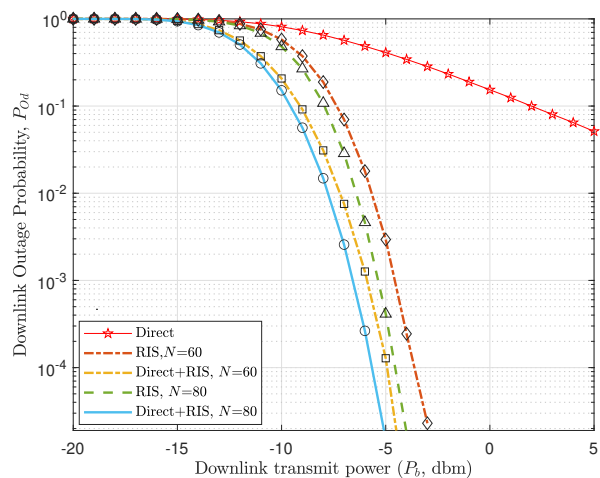


Fig. 10: Outage probability at DCU vs downlink power.

dBm, respectively. In addition to this, one can also observe a significant increase in  $G_d$  with an increase in  $N$  for the RIS-only and Direct+RIS cases.

## B. Results for IBL transmission

### 1) Uplink Communication

Fig. 8 exhibits the outage probability plotted against the total transmit power available at UCU. It compares the outage probability at the AP during uplink transmission with all three cases considering IBL transmission. The close proximity between the analytical and simulated results proves the accuracy of the derived expression for the outage probability in (52). It can be seen that, due to an increase in SINR, the outage probability decreases with an increase in transmit power at UCU. Further, as evident from the figure, the outage probability for RIS-case is lower than the outage probability for Direct-case. Therefore, the use of RIS enhances the performance of the considered system as compared to the Direct-only case with IBL transmission. It can also be observed that the outage

probability is further reduced for the Direct+RIS case, thus outperforming the other two cases.

Fig. 9 exhibits the throughput plotted against the total transmit power available at UCU for different numbers of reflecting elements at the RIS  $R_u$ . It can be observed that the throughput increases as the transmit power available at UCU increases, however, the throughput converges to a constant value when the SINR reaches a particular value. Also, the throughput increases dramatically with increasing  $K$ . The close proximity between analytical and simulated graphs proves the accuracy of the throughput expression (55).

### 2) Downlink Communication

Fig. 10 depicts the outage probability at DCU during the downlink transmission w.r.t. the available transmit power at the AP for all three cases. As expected, the close proximity between analytical and simulated curves proves the accuracy of the derived expression for the outage probability in (57). Also, similar to the previous figure, the outage probability decreases with increasing transmit power at the AP, and the outage probability for the RIS-only case is better than that

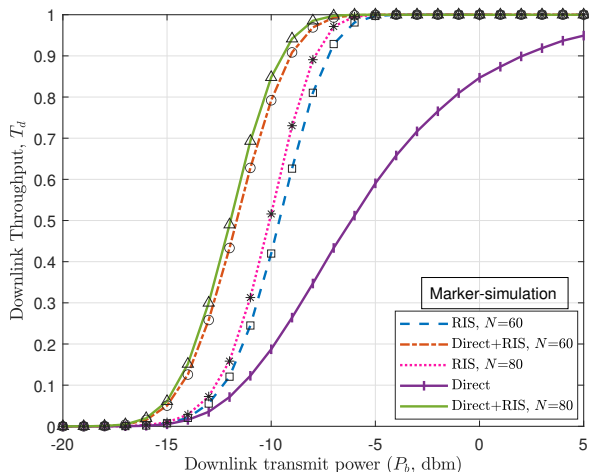


Fig. 11: Throughput at DCU vs power at AP.

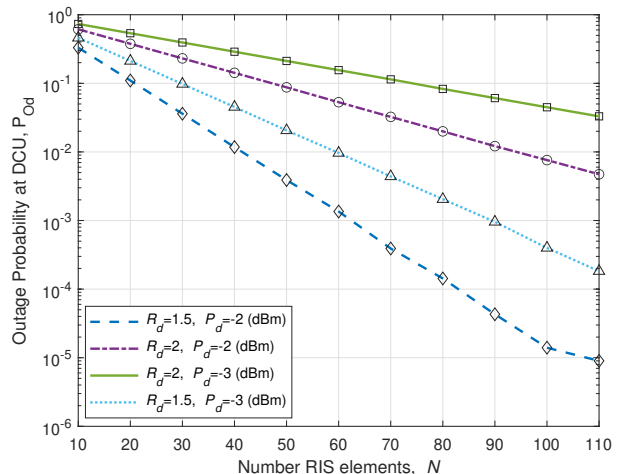


Fig. 13: Outage probability at DCU vs number of RIS elements.

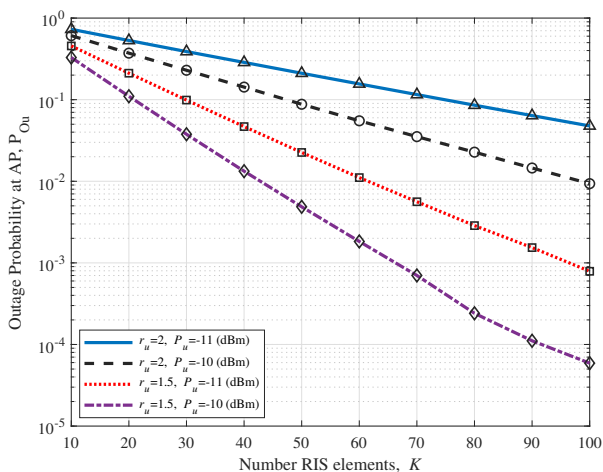


Fig. 12: Outage probability at AP vs number of RIS elements.

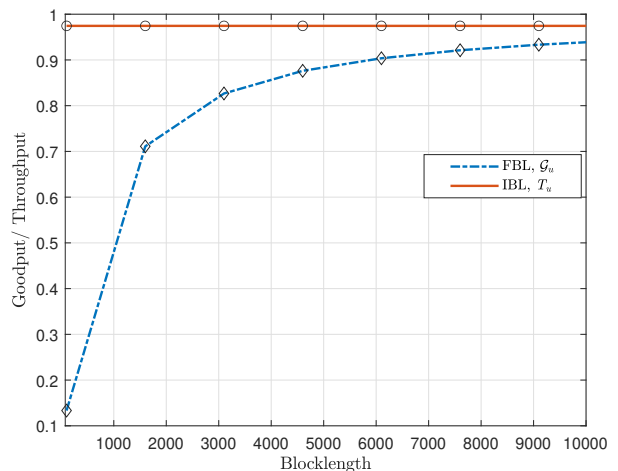


Fig. 14: Infinite and finite block length transmission.

for the Direct-only case. The outage probability is further enhanced for the Direct+RIS case. Additionally, the outage probability of the DCU is much lower than that of the UCU despite the increase in the distance between AP- $R_d$  and  $R_d$ -DCU, this is because of the high transmit power available at the AP and the number of RIS elements considered in RIS- $R_d$ .

Fig. 11 shows the system throughput at the DCU during the downlink transmission w.r.t. available transmit power at the AP obtained for all three cases discussed in the previous figure. As expected, the close proximity between analytical and simulated curves validates the accuracy of the throughput expression (60). At low transmit power, the throughput of the system corresponding to the higher target rates is very low, but as the power increases the system throughput also increases. Subsequently, after a specific value of transmit power the throughput saturates and yields the maximum achievable throughput for the considered range. Moreover, it can be observed that the system throughput for the RIS-only case is better than that of the Direct-only case. Additionally, the throughput is further enhanced for the Direct+RIS case. Furthermore, to highlight

the impact of the number of RIS elements on the outage behaviour, we plot the outage performance at the AP during uplink transmission versus the number of RIS elements  $K$  at  $R_u$  in Fig. 12, and the outage performance at DCU during downlink transmission versus the number of RIS elements  $N$  at  $R_d$  in Fig. 13. For uplink transmission, it is obtained for different values of the transmit power  $P_u$  available at UCU and the target rate at AP. As can be observed, due to the increase in diversity, the outage probability improves with increasing  $K$ . However, because of the increase in the SINR threshold, the outage probability degrades with an increase in the target rate at the AP. The outage probability at DCU also follows the same behaviour w.r.t.  $N$  at  $R_d$ . Thus, depending on the QoSs and available power, one can always choose an appropriate number of elements at each RIS.

### C. Comparison of IBL and FBL transmission

Fig. 14 compares the IBL and FBL transmission network performance which is obtained by plotting throughput ( $T_u$ ) and goodput ( $G_u$ ) with respect to blocklength. It can be observed

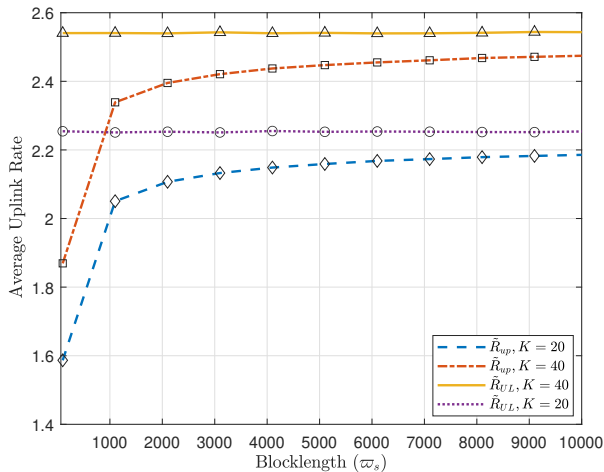


Fig. 15: Average Uplink rate vs blocklength.

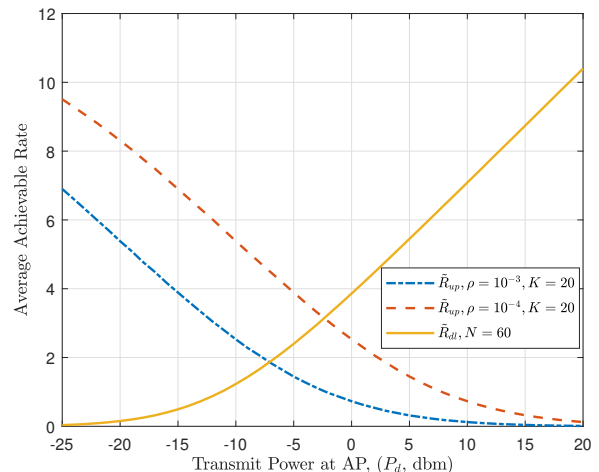


Fig. 17: Achievable rate vs transmit power at AP.

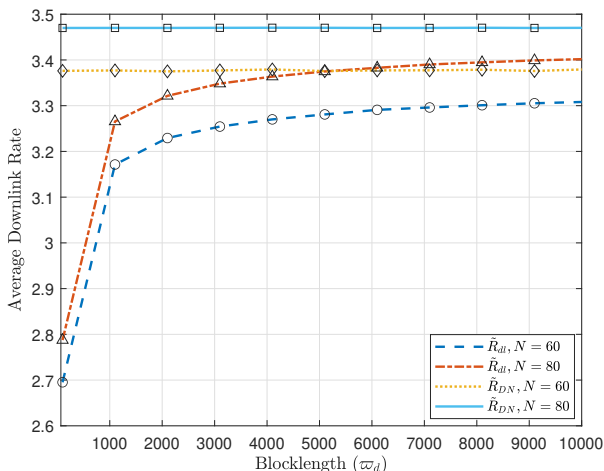


Fig. 16: Average downlink rate vs blocklength.

that  $\mathcal{G}_u$  increases with increasing blocklength. Additionally,  $\mathcal{G}_u$  approaches  $T_u$  as blocklength tends to infinity. However, in contrast to the IBL analysis, the FBL analysis captures the more realistic performance estimates for short packet transmission (i.e., low-latency communication).

#### D. Achievable rate results

Fig. 15 shows the average achievable rate at the AP during uplink communication for FBL and IBL transmissions. It is obtained by plotting  $\tilde{R}_{up}$  and  $\tilde{R}_{UL}$  w.r.t. blocklength for different numbers of elements  $K$  at  $R_u$  with  $P_u = -11$  dBm. The close agreement between the simulated and analytical graphs validates the accuracy of the derived expressions in (64) and (66). It can be observed that  $\tilde{R}_{up}$  increases with an increase in  $\varpi_s$ , whereas  $\tilde{R}_{UL}$  is constant throughout the range of  $\varpi_s$ . Additionally,  $\tilde{R}_{up} \rightarrow \tilde{R}_{UL}$  as  $\varpi_s$  increases.

Similar to Fig. 15, Fig. 16 depicts the average downlink achievable rate for FBL and IBL transmissions which is obtained by plotting  $\tilde{R}_{dl}$  and  $\tilde{R}_{DN}$  w.r.t.  $\varpi_d$  for the different numbers of reflecting elements  $N$  at  $R_d$  with  $P_d = -2$  dBm.

The graph validates the accuracy of the derived expressions in (69) and (70) and the simulated results. As we increase  $\varpi_d$ ,  $\tilde{R}_{dl}$  also increases, whereas  $\tilde{R}_{DN}$  remains constant throughout the range of  $\varpi_d$ . However, it can be observed that  $\tilde{R}_{dl} \rightarrow \tilde{R}_{DN}$  as  $\varpi_d$  increases.

Fig. 17 depicts the average achievable rate of uplink ( $\tilde{R}_{up}$ ) and downlink ( $\tilde{R}_{dl}$ ) transmission plotted for FBL transmission w.r.t. transmit power ( $P_d$ ) at the AP for different values of SI cancellation factor ( $\rho$ ) with  $P_u = 17$  dBm and  $\varpi_d = \varpi_s = 3000$ . As expected,  $\tilde{R}_{dl}$  increases with an increase in  $P_d$  whereas, due to the imperfection in SI cancellation ( $\rho \neq 0$ ),  $\tilde{R}_{up}$  decreases for the same context. In addition to this, one can also notice the decrease in  $\tilde{R}_{up}$  with an increase in  $\rho$ . For example,  $\tilde{R}_{up} \approx 7$  when  $\rho = 10^{-4}$  whereas  $\tilde{R}_{up} \approx 4$  when  $\rho = 10^{-3}$  at  $-15$  dBm. Therefore, there is a trade-off between the uplink and downlink rates because of the SI at the AP. Thus, for achieving the desired QoS, a judicious choice of transmit power at the AP is very important.

#### E. Impact of imperfect CSI

As discussed earlier, we have considered perfect CSI for analytical tractability. However, in order to provide some useful insights, in Fig. 18 we demonstrate the impact of imperfect CSI on the achievable throughput ( $T_u$ ) for different transmit power available at UCU and for different values of  $\delta_u$  and  $K$ . As expected, the throughput is maximum when there is no CSI error. However, there is a significant decrease in throughput with an increase in  $\delta_u$ . For instance, for perfect CSI, i.e.,  $\delta_u = 0$ ,  $T_u \approx 0.78$  at  $P_u = -15$  dBm with  $K = 20$ , whereas  $T_u \approx 0.69$  for  $\delta_u = 0.1$  and  $T_u \approx 0.61$  for  $\delta_u = 0.2$  at  $P_u = -15$  dBm with  $K = 20$ . Interestingly,  $T_u$  at  $K = 60$  and  $\delta_u = 0.2$  is still greater than  $T_u$  at  $K = 20$  and  $\delta_u = 0$ . Thus, one can always increase the number of elements at the RIS to achieve the desired QoS in the presence of imperfect CSI.

Similar to the previous figure, Fig. 19 shows the impact of imperfect CSI on the achievable downlink throughput ( $T_d$ ) for various transmit power available at the AP for different values

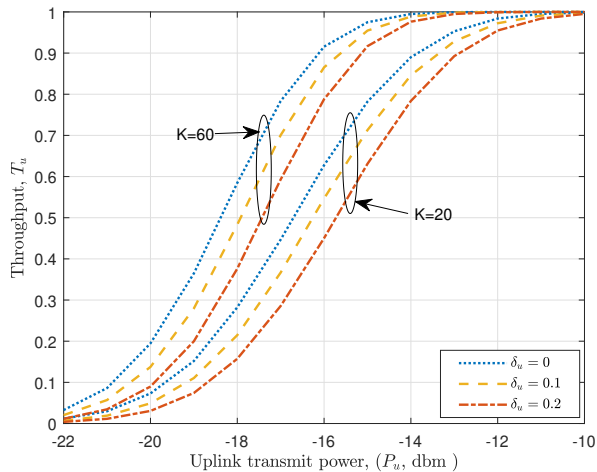


Fig. 18: Impact of imperfect CSI on uplink throughput.

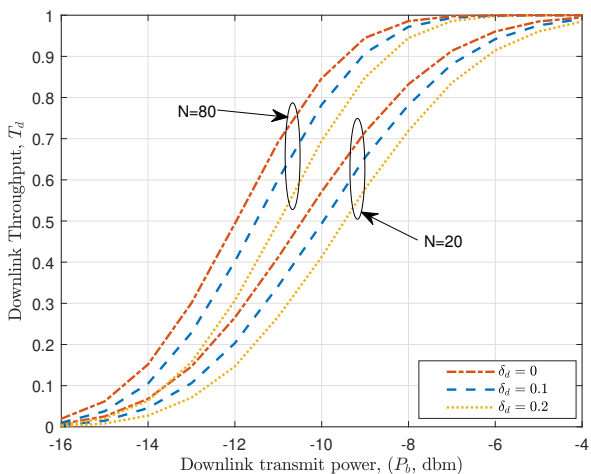


Fig. 19: Impact of imperfect CSI on downlink throughput.

of  $\delta_d$  and  $N$ . It can be observed that the system performance degrades as the imperfection  $\delta_d$  increases. For example, at  $-10$  dBm with  $\delta_d = 0.2$ , the system has an achievable  $T_d \approx 0.4$  for  $N = 20$ . However, when  $N = 80$  and  $\delta_d = 0.2$ , the system has an achievable  $T_d \approx 0.7$ . This indicates that a judicious choice of RIS elements can help in achieving the desired QoS in the presence of CSI estimation error.

#### F. NOMA-enhanced Multi-user Communication

For the multi-user case, in our simulations all of the users are assumed to be distributed within a distance of  $50 - 70$  m from the AP and  $5 - 15$  m from the respective RIS, while all other parameters are considered to be the same as in the single user case. Moreover, the devices in each link are considered to be on either side of the AP in order to avoid interference, and optimum power coefficient allocation is obtained using an exhaustive search algorithm [51]. Fig. 20 and Fig. 21 depict the variation of the outage probability for downlink and uplink transmission, respectively, considering two uplink and two downlink users. Fig. 20 is obtained by plotting the

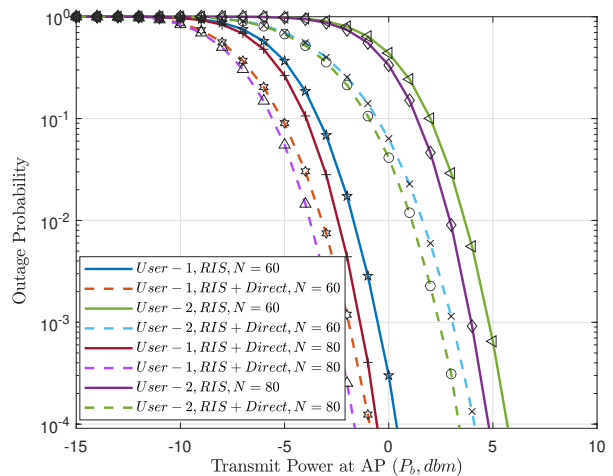


Fig. 20: Multi-user downlink outage probability

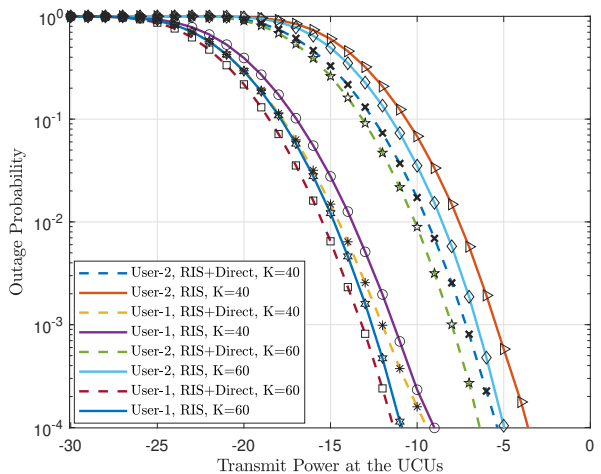


Fig. 21: Multi-user uplink outage probability

outage probability at each DCU w.r.t. transmit power ( $P_b$ ) at the AP for RIS-only and Direct+RIS cases. As expected, the close proximity between analytical and simulated curves demonstrates the accuracy of the derived expression (76) for the outage probability. It can be observed that the outage probability decreases with an increase in transmit power at the AP for both cases. However, due to higher SINR, Direct+RIS provides better performance compared to the RIS-only case. Moreover, as the number of reflecting elements  $N$  is increased, the outage probability decreases. A similar behaviour can also be observed in Fig. 21, which is obtained by plotting outage probability at the AP corresponding to each UCU symbol w.r.t. transmit power at each UCU, i.e., ( $P_{u1} = P_{u2}$ ).

The average BLER for the DCUs is plotted in Fig. 22 by varying  $P_b$ . Similar to Fig. 20, it can be observed that, due to an increase in net SINR, the average achievable BLER improves as the transmit power at the AP increases. The simulation results are in close agreement with the BLER expression derived in (44), which proves the accuracy of the derived analytical expression. It can be observed that the

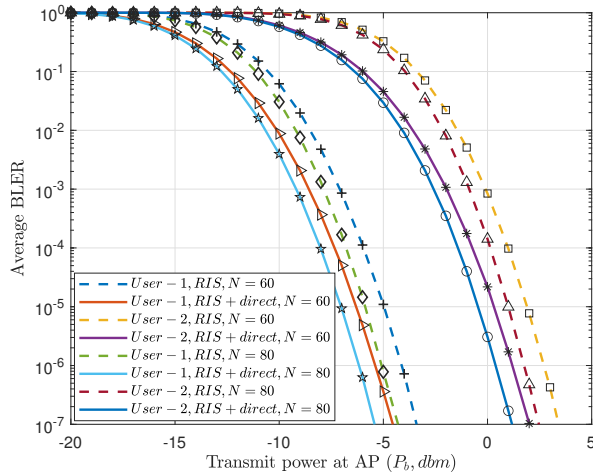


Fig. 22: Multi-user downlink BLER

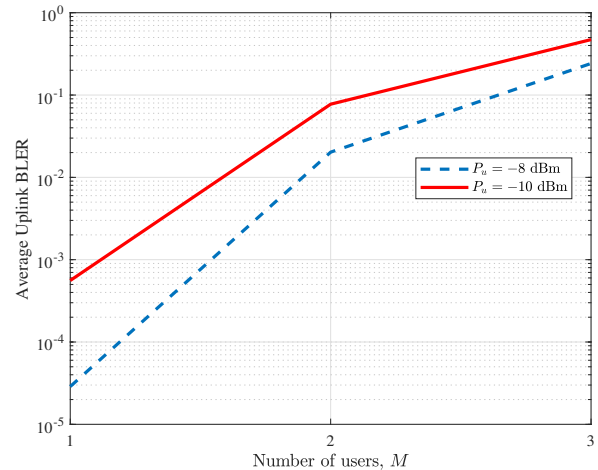


Fig. 24: Impact of number of UCU on Uplink BLER

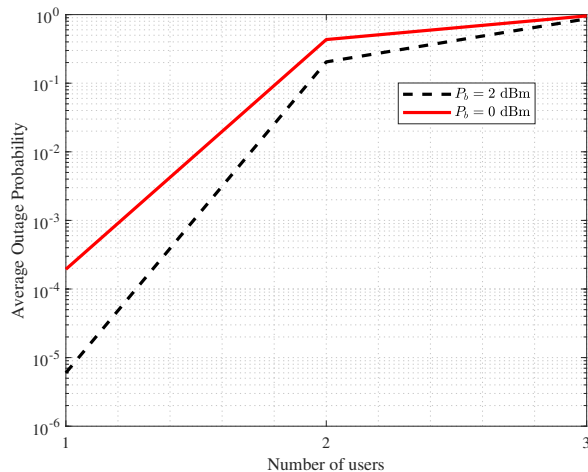


Fig. 23: Impact of number of DCU on downlink AOP

use of the RIS can provide a significant improvement in the achievable BLER for the downlink communication.

We highlight the impact of the number of DCUs on the *average outage probability* (AOP) of the downlink transmission, which is defined as  $P_{d,avg} = (1/L) \sum_{l=1}^L P_{Odl}$ , in Fig. 23. It can be seen that the AOP of downlink transmission increases with increasing  $L$ . This behaviour of the AOP is due to the increase in inter-user interference at each user that leads to a reduction in net SINR for SIC and user symbol decoding, which in turn increases the probability of outage at each user. Further, it can also be noted that there is an improvement in performance with an increase in  $P_b$ . Similarly, we highlight the impact of the number of UCUs on the average BLER at the AP during uplink transmission in Fig. 24. Clearly, the observations are similar to Fig. 23. Thus, we can say that higher transmit power at each device allows the system to accommodate more users in each link.

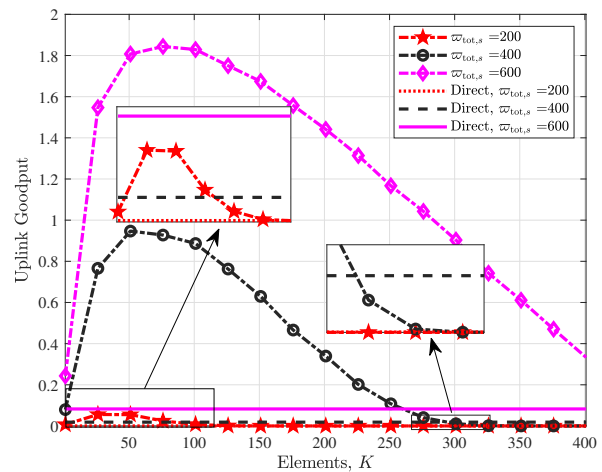


Fig. 25: Impact of training overhead

### G. Impact of Training Overhead

Finally, we show the impact of training overhead on the goodput performance of the considered network in Fig. 25. It is obtained by plotting the uplink goodput ( $\mathcal{G}_u$ ) versus the number of reflecting elements ( $K$ ) at the RIS with  $P_u = -25$  dBm and  $r_u = 3$  for different values of  $\varpi_{tot,s}$ . Further, for simplicity, we assume that  $\varpi_{train,s} = K + 1$  for obtaining  $K$  cascaded UCU-RIS-AP channels and one direct path channel (UCU-AP), and thus  $\varpi_s = \varpi_{tot,s} - (K + 1)$ . It can be seen that at first, due to passive beamforming gain, there is a significant increase in  $\mathcal{G}_u$  with increasing  $K$ . However,  $\mathcal{G}_u$  reaches a peak value after a certain  $K$  and thereafter decreases significantly with increasing  $K$ . The main reason for this behaviour is the high value of  $\varpi_{train,s}$  for higher  $K$  leading to a significant decrease in  $\varpi_s$ , which in turn decreases  $\mathcal{G}_u$ . For example, for  $\varpi_{tot,s} = 400$ ,  $\mathcal{G}_u$  increases from 0.1 to 0.9 when  $K$  increases from 1 to 50 whereas  $\mathcal{G}_u$  decrease from 0.9 to less than 0.1 when  $K$  increases from 50 to less than 250. It can also be noted that due to the increased training overhead, the goodput  $\mathcal{G}_u$  eventually becomes lower than that

of the Direct-only case. In such cases, where  $\varpi_{\text{tot},s}$  is limited, the use of a large number of elements at the RIS is not justified. Therefore, in such cases, one needs to choose an optimum value of the number of RIS elements to maximize the performance. However, it can be seen that a higher  $\varpi_{\text{tot},s}$  allows the system to support larger values of  $K$ . For example, the peak value of  $\mathcal{G}_u$  is obtained at  $K = \{45, 50, 70\}$  when  $\varpi_{\text{tot},s} = \{200, 400, 600\}$ , respectively. The main reason for this is the fact that after fixing  $\varpi_{\text{train},s}$ , higher  $\varpi_{\text{tot},s}$  will assign higher  $\varpi_s$  ( $\varpi_s \gg \varpi_{\text{train},s}$ ), hence alleviating the impact of training overhead.

### VIII. CONCLUSIONS

In this paper, the performance analysis of an RIS-aided FD communication network consisting of an FD-AP that communicates with an uplink and a downlink cellular user simultaneously presented for the case of infinite and finite blocklength. We analyzed the performance of the considered system by deriving closed-form expressions for the outage probability, throughput, BLER and goodput, calculated the maximum achievable rate for FBL and IBL transmission for both uplink and downlink communications, and validated their accuracy using Monte-Carlo simulation. Further, based on the single-user framework, we extended the analysis to a more practical case with multiple users utilizing NOMA on each link and derived the analytical expressions for the outage probability and BLER at each downlink user and at the AP. Through comparative analysis, we have highlighted the performance gains achievable through the use of the RIS in FD communication. We also demonstrated the impact of the transmit power at the AP on the performance of uplink communication and showed why it is extremely important to use an appropriate transmit power during downlink communication in order to attain desired performance in uplink communication. We also highlighted how a judicious choice of the number of RIS elements can help to achieve the desired QoS in the presence of CSI estimation error. Such a mathematical framework can aid in the design of efficient and reliable RIS-aided FD networks for future wireless applications. An interesting direction for future work is an extension of this work to a more general case where each device has multiple antennas.

### REFERENCES

- [1] Y. Liu, X. Wang, G. Boudreau, A. B. Sediq, and H. Abou-Zeid, "A multi-dimensional intelligent multiple access technique for 5G beyond and 6G wireless networks," *IEEE Trans. Wireless Commun.*, vol. 20, no. 2, pp. 1308–1320, Oct. 2021.
- [2] L. Wei *et al.*, "Multi-user holographic MIMO surfaces: Channel modeling and spectral efficiency analysis," *IEEE J. Sel. Top. Signal Process.*, vol. 16, no. 5, pp. 1112–1124, Aug. 2022.
- [3] Q. Wu and R. Zhang, "Intelligent reflecting surface enhanced wireless network: Joint active and passive beamforming design," in *IEEE GLOBECOM*, Abu Dhabi, United Arab Emirates, Feb. 2018, pp. 1–6.
- [4] H. Zhang, H. Zhang, B. Di, K. Bian, Z. Han, and L. Song, "Towards ubiquitous positioning by leveraging reconfigurable intelligent surface," *IEEE Commun. Lett.*, vol. 25, no. 1, pp. 284–288, Sep. 2020.
- [5] J. Lyu and R. Zhang, "Hybrid active/passive wireless network aided by intelligent reflecting surface: System modeling and performance analysis," *IEEE Trans. Wireless Commun.*, vol. 20, pp. 7196–7212, Nov. 2021.
- [6] C. Huang *et al.*, "Multi-hop RIS-empowered terahertz communications: A DRL-based hybrid beamforming design," *IEEE J. Sel. Areas Commun.*, vol. 39, no. 6, pp. 1663–1677, Jun. 2021.
- [7] S. Zhang and R. Zhang, "Capacity characterization for intelligent reflecting surface aided MIMO communication," *IEEE J. Sel. Areas Commun.*, vol. 38, pp. 1823–1838, Aug. 2020.
- [8] M. A. Kishk and M.-S. Alouini, "Exploiting randomly located blockages for large-scale deployment of intelligent surfaces," *IEEE J. Sel. Areas Commun.*, vol. 39, pp. 1043–1056, Apr. 2021.
- [9] H. Lu, Y. Zeng, S. Jin, and R. Zhang, "Aerial intelligent reflecting surface: Joint placement and passive beamforming design with 3D beam flattening," *IEEE Trans. Wireless Commun.*, vol. 20, pp. 4128–4143, Jul. 2021.
- [10] M. H. N. Shaikh, V. A. Bohara, and A. Srivastava, "Performance analysis of a full-duplex MIMO decode-and-forward relay system with self-energy recycling," *IEEE Access*, vol. 8, pp. 226 248–226 266, Dec. 2020.
- [11] K. Singh, S. Biswas, M.-L. Ku, and M. F. Flanagan, "Transceiver design and power control for full-duplex ultra-reliable low-latency communication systems," *IEEE Trans. Wireless Commun.*, vol. 21, no. 2, pp. 1392–1406, Feb. 2022.
- [12] B. C. Nguyen, T. M. Hoang, L. T. Dung, and T. Kim, "On performance of two-way full-duplex communication system with reconfigurable intelligent surface," *IEEE Access*, vol. 9, pp. 81 274–81 285, Jun. 2021.
- [13] S. Dhok, P. Raut, P. K. Sharma, K. Singh, and C.-P. Li, "Non-linear energy harvesting in RIS-assisted URLLC networks for industry automation," *IEEE Trans. Commun.*, vol. 69, no. 11, pp. 7761–7774, Nov. 2021.
- [14] A. Faisal, I. Al-Nahhal, O. A. Dobre, and T. M. N. Ngatched, "Deep reinforcement learning for optimizing RIS-assisted HD-FD wireless systems," *IEEE Commun. Lett.*, vol. 25, no. 12, pp. 3893–3897, Dec. 2021.
- [15] P. K. Sharma and P. Garg, "Intelligent reflecting surfaces to achieve the full-duplex wireless communication," *IEEE Commun. Lett.*, vol. 25, no. 2, pp. 622–626, Oct. 2020.
- [16] A. Bansal, K. Singh, and C.-P. Li, "Analysis of hierarchical rate splitting for intelligent reflecting surfaces-aided downlink multiuser MISO communications," *IEEE Open J. Commun. Soc.*, vol. 2, pp. 785–798, Apr. 2021.
- [17] W. Mei and R. Zhang, "Performance analysis and user association optimization for wireless network aided by multiple intelligent reflecting surfaces," *IEEE Trans. Commun.*, vol. 69, no. 9, pp. 6296–6312, Jun. 2021.
- [18] F. Karim, B. Hazarika, S. K. Singh, and K. Singh, "A performance analysis for multi-RIS-assisted full duplex wireless communication system," in *Proc. IEEE ICASSP*, Singapore, May 2022.
- [19] Q. Tao, J. Wang, and C. Zhong, "Performance analysis of intelligent reflecting surface aided communication systems," *IEEE Commun. Lett.*, vol. 24, pp. 2464–2468, Nov. 2020.
- [20] L. Yang, F. Meng, M. O. Hasna, and E. Basar, "A novel RIS-assisted modulation scheme," *IEEE Wireless Commun. Lett.*, vol. 10, no. 6, pp. 1359–1363, Jun. 2021.
- [21] H. Alves, G. D. Jo, J. Shin, C. I. Yeh, N. H. Mahmood, C. H. M. de Lima, C. Yoon, N. Rajatheva, O. Park, S. Kim, E. Kim, V. Niemelä, H. W. Lee, A. Pouttu, H. K. Chung, and M. Latva-aho, "Beyond 5G URLLC evolution: New service modes and practical considerations," *CoRR*, vol. abs/2106.11825, 2021. [Online]. Available: <https://arxiv.org/abs/2106.11825>
- [22] G. Brown *et al.*, "Ultra-reliable low-latency 5G for industrial automation," *Technol. Rep. Qualcomm*, vol. 2, p. 52065394, 2018. [Online]. Available: <https://www.qualcomm.com/media/documents/files/read-the-white-paper-by-heavy-reading.pdf>
- [23] B. Makki, T. Svensson, and M. Zorzi, "Wireless energy and information transmission using feedback: Infinite and finite block-length analysis," *IEEE Trans. Commun.*, vol. 64, pp. 5304–5318, Dec. 2016.
- [24] Z. Zheng, L. Yuan, and F. Fang, "Performance analysis of fountain coded non-orthogonal multiple access with finite blocklength," *IEEE Wireless Commun. Lett.*, vol. 10, no. 8, pp. 1752–1756, Aug. 2021.
- [25] P. Raut, K. Singh, C. Li, M. Alouini, and W. Huang, "Nonlinear EH-based UAV-assisted FD IoT networks: Infinite and finite blocklength analysis," *IEEE Internet Things J.*, vol. 8, no. 24, pp. 17 655–17 668, Dec. 2021.
- [26] Y. Hu, J. Gross, and A. Schmeink, "On the performance advantage of relaying under the finite blocklength regime," *IEEE Commun. Lett.*, vol. 19, no. 5, pp. 779–782, May 2015.
- [27] C. Feng, H.-M. Wang, and H. V. Poor, "Reliable and secure short-packet communications," *IEEE Trans. Wireless Commun.*, vol. 21, no. 3, pp. 1913–1926, Mar. 2022.

- [28] D. Tran *et al.*, “Short-packet communications for MIMO NOMA systems over Nakagami-m fading: BLER and minimum blocklength analysis,” *IEEE Trans. Veh. Technol.*, vol. 70, no. 4, pp. 3583–3598, Apr. 2021.
- [29] Y. Cai, M.-M. Zhao, K. Xu, and R. Zhang, “Intelligent reflecting surface aided full-duplex communication: Passive beamforming and deployment design,” *IEEE Trans. Wireless Commun.*, vol. 21, no. 1, pp. 383–397, Jan. 2022.
- [30] E. Björnson and L. Sanguinetti, “Rayleigh fading modeling and channel hardening for reconfigurable intelligent surfaces,” *IEEE Wireless Commun. Lett.*, vol. 10, no. 4, pp. 830–834, Apr. 2021.
- [31] R. Zhong, Y. Liu, X. Mu, Y. Chen, and L. Song, “AI empowered RIS-assisted NOMA networks: Deep learning or reinforcement learning?” *IEEE J. Sel. Areas Commun.*, vol. 40, no. 1, pp. 182–196, Jan. 2022.
- [32] Y. Cheng, K. H. Li, Y. Liu, K. C. Teh, and H. V. Poor, “Downlink and uplink intelligent reflecting surface aided networks: NOMA and OMA,” *IEEE Trans. Wireless Commun.*, vol. 20, pp. 3988–4000, Feb. 2021.
- [33] D. Selimis, K. P. Peppas, G. C. Alexandropoulos, and F. I. Lazarakis, “On the performance analysis of RIS-empowered communications over Nakagami-m fading,” *IEEE Commun. Lett.*, vol. 25, no. 7, pp. 2191–2195, Jul. 2021.
- [34] R. C. Ferreira, M. S. P. Facina, F. A. P. de Figueiredo, G. Fraidenraich, and E. R. de Lima, “Bit error probability for large intelligent surfaces under double-Nakagami fading channels,” *IEEE Open J. Commun. Soc.*, vol. 1, pp. 750–759, May 2020.
- [35] C. Zhang, W. Yi, Y. Liu, K. Yang, and Z. Ding, “Reconfigurable intelligent surfaces aided multi-cell NOMA networks: A stochastic geometry model,” *IEEE Trans. Commun.*, vol. 70, no. 2, pp. 951–966, Feb. 2022.
- [36] G. Taricco, “Series expansions and approximations of the Nakagami-m sum probability density function,” *IEEE Wireless Commun. Lett.*, vol. 11, no. 1, pp. 160–164, Jan. 2022.
- [37] L. Wei, C. Huang, G. C. Alexandropoulos, C. Yuen, Z. Zhang, and M. Debbah, “Channel estimation for RIS-empowered multi-user MISO wireless communications,” *IEEE Trans. Commun.*, vol. 69, no. 6, pp. 4144–4157, Jun. 2021.
- [38] H. Zhang, B. Di, Z. Han, H. V. Poor, and L. Song, “Reconfigurable intelligent surface assisted multi-user communications: How many reflective elements do we need?” *IEEE Wireless Commun. Lett.*, vol. 10, no. 5, pp. 1098–1102, May 2021.
- [39] A. Sabharwal, P. Schniter, D. Guo, D. W. Bliss, S. Rangarajan, and R. Wichman, “In-band full-duplex wireless: Challenges and opportunities,” *IEEE J. Sel. Areas Commun.*, vol. 32, no. 9, pp. 1637–1652, Jun. 2014.
- [40] Z. Zhang, X. Chai, K. Long, A. V. Vasilakos, and L. Hanzo, “Full duplex techniques for 5G networks: self-interference cancellation, protocol design, and relay selection,” *IEEE Commun. Mag.*, vol. 53, no. 5, pp. 128–137, May 2015.
- [41] E. Basar, M. Di Renzo, J. De Rosny, M. Debbah, M.-S. Alouini, and R. Zhang, “Wireless communications through reconfigurable intelligent surfaces,” *IEEE Access*, vol. 7, pp. 116 753–116 773, Aug. 2019.
- [42] E. Björnson, O. Ozdogan, and E. G. Larsson, “Intelligent reflecting surface versus decode-and-forward: How large surfaces are needed to beat relaying?” *IEEE Wireless Commun. Lett.*, vol. 9, no. 2, pp. 244–248, Oct. 2020.
- [43] I. S. Gradshteyn *et al.*, *Table of Integrals, Series, and Products*, 7th ed. San Diego, CA, USA: Academic Press, 2007.
- [44] B. Tahir, S. Schwarz, and M. Rupp, “Analysis of uplink IRS-assisted NOMA under Nakagami-m fading via moments matching,” *IEEE Wireless Commun. Lett.*, vol. 10, no. 3, pp. 624–628, Mar. 2021.
- [45] A. Papoulis, *Random variables and stochastic processes*. McGraw Hill, 1994.
- [46] M. Abramowitz *et al.*, “Handbook of mathematical functions with formulas, graphs and mathematical tables,” 1972.
- [47] Y. Hu, A. Schmeink, and J. Gross, “Blocklength-limited performance of relaying under quasi-static Rayleigh channels,” *IEEE Trans. Wireless Commun.*, vol. 15, no. 7, pp. 4548–4558, Jul. 2016.
- [48] Y. Polyanskiy, H. V. Poor, and S. Verdú, “Channel coding rate in the finite blocklength regime,” *IEEE Trans. Inf. Theory*, vol. 56, no. 5, pp. 2307–2359, May 2010.
- [49] Y. Gu, H. Chen, Y. Li, and B. Vucetic, “Ultra-reliable short-packet communications: Half-duplex or full-duplex relaying?” *IEEE Wireless Commun. Lett.*, vol. 7, no. 3, pp. 348–351, Jun. 2018.
- [50] T. H. Vu *et al.*, “Short-packet communications for UAV-based NOMA systems under imperfect CSI and SIC,” *IEEE Trans. Cogn. Commun. Netw.*, pp. 1–1, Nov. 2022.
- [51] S. K. Singh, K. Agrawal, K. Singh, C.-P. Li, and Z. Ding, “NOMA enhanced hybrid RIS-UAV-assisted full-duplex communication system with imperfect SIC and CSI,” *IEEE Trans. Commun.*, pp. 1–1, Oct. 2022.
- [52] B. Zheng, C. You, and R. Zhang, “Uplink channel estimation for double-IRS assisted multi-user MIMO,” in *Proc. IEEE ICC*, Montreal, QC, Canada, Jun. 2021, pp. 1–6.



**Keshav Singh (Member, IEEE)** received the M.Sc. degree in Information and Telecommunications Technologies from Athens Information Technology, Greece, in 2009, and the Ph.D. degree in Communication Engineering from National Central University, Taiwan, in 2015. He currently works at the Institute of Communications Engineering, National Sun Yat-sen University (NSYSU), Taiwan as an Assistant Professor. Prior to this, he held the position of Research Associate from 2016 to 2019 at the Institute of Digital Communications, University of Edinburgh, U.K. From 2019 to 2020, he was associated with the University College Dublin, Ireland as a Research Fellow. He leads research in the areas of green communications, resource allocation, transceiver design for full-duplex radio, ultra-reliable low-latency communication, non-orthogonal multiple access, wireless edge caching, machine learning for wireless communications, and large intelligent surface assisted communications.



**Farjam Karim** is a recent graduate holding Masters of Science degree in Telecommunications Engineering from National Sun Yat-sen University, Taiwan. His research interests include Full duplex technologies, Reconfigurable Intelligent Surfaces, STAR-RISs, Non Orthogonal Multiple access, Rate Spilling Multiple access and Performance Analysis for Short packet communications.



**Sandeep Kumar Singh (Member, IEEE)** received his B.E. degree in Electronics and Communication Engineering from RGPV University, Bhopal, India in 2010, M.Tech. degree in ME and VLSI Design from MNNIT Allahabad, Prayagraj, India in 2013, and Ph.D. degree in Electronics and Communication Engineering from VNIT Nagpur, India in 2020. He is currently a post-doctoral researcher at the Institute of Communications Engineering, National Sun Yat-sen University (NSYSU), Taiwan. His current research interests are in the areas of RSMA, NOMA, UAV, RIS/IRS, wireless energy harvesting, Massive MIMO, full-duplex radio, and OFDM.



**Prabhat Kumar Sharma (Senior Member, IEEE)**

received the B.Tech. and M.Tech. degrees in electronics and communication engineering and VLSI design from Uttar Pradesh Technical University, Lucknow, and Malaviya National Institute of Technology, Jaipur, respectively, and the Ph.D. degree in wireless communications from the University of Delhi in 2015. He is an Assistant Professor with the Department of Electronics and Communication Engineering, Visvesvaraya National Institute of Technology, Nagpur, India. He has authored over

80 journal and conference papers. His current research interests include Molecular and Biological Communications, and 6G and Beyond Wireless Communications Systems. He is recipient of the Visvesvaraya Young Faculty Research Fellowship from the Ministry of Electronics and Information Technology, Government of India, and URSI/InRaSS Young Indian Radio Scientist Award 2019. Dr. Sharma is currently serving on the editorial boards of IEEE Transactions of Molecular Biological and Multiscale communications and IEEE Wireless Communication letters.



**Shahid Mumtaz (Senior Member, IEEE)** is a Nottingham Trent University (NTU), UK professor. He is an IET Fellow, founder, and EiC of IET "Journal of Quantum Communication," Vice-Chair: Europe/Africa Region- IEEE ComSoc: Green Communications & Computing Society. He authorizes four technical books, 12 book chapters, and 300+ technical papers (200+ IEEE Journals/transactions, 100+ conferences, 2 IEEE best paper awards) in mobile communications. Most of his publication is in the field of Wireless Communication. He is a

Scientific Expert and Evaluator for various research funding agencies. In 2012, he was awarded an "Alain Bensoussan fellowship." China awarded him the young scientist fellowship in 2017.



**Mark F. Flanagan (Senior Member, IEEE)** received the B.E. and Ph.D. degrees in electronic engineering from University College Dublin (UCD), Dublin, Ireland, in 1998 and 2005, respectively. He is currently a Professor with the School of Electrical and Electronic Engineering, UCD, having been first appointed as SFI Stokes Lecturer in 2008. Prior to this, he held post-doctoral research fellowship positions with the University of Zurich, Switzerland, the University of Bologna, Italy, and the University of Edinburgh, U.K. In 2014, he was a Visiting Senior

Scientist with the Institute of Communications and Navigation, German Aerospace Center, Munich, under a DLR-DAAD Fellowship. He has published more than 150 papers in peer-reviewed international journals and conferences. His research interests broadly span wireless communications, coding and information theory, and signal processing. He was a recipient of the Stokes Lectureship Award from Science Foundation Ireland (SFI) in 2008 and the Consolidator Laureate Award from the Irish Research Council (IRC) in 2018. He was a recipient of the Best Paper Award at Globecom 2021. He served as TPC Co-Chair for the Communication Theory Symposium at IEEE ICC 2020 and at IEEE GLOBECOM 2022. He is currently serving as TPC Co-Chair for the Wireless Communications Symposium at IEEE ICC 2024. He is also serving as Secretary of the IEEE Radio Communications Society and as Vice-Chair for the Special Interest Group on Reconfigurable Intelligent Surfaces of the Signal Processing and Computing for Communications (SPCC) Technical Committee of the IEEE Communications Society. During the period 2012–2021 he served in the roles of Editor, Senior Editor, and Executive Editor for IEEE Communications Letters. He is currently serving as an Editor for IEEE Transactions on Communications.